Experimental Reports

(2017)

Activity Report on Neutron Scattering Research: Experimental Reports Vol. 23 (2017)

Published by:
Neutron Science Laboratory,
Institute for Solid State Physics,
University of Tokyo
106-1, Shirakata, Tokai,
Ibaraki 319-1106,
JAPAN

This volume contains experimental reports submitted in the following period of time: 2017/06/22 to 2018/07/31.
Visit our on-line database for updated information.

Structures and Excitations

Magnetism

- Magnetic diffuse scattering in pyrochlore antiferromagnet Na3Mn(CO3)2Cl
  K. Nawa, D. Okuyama, M. Avdeev, and T. J. Sato
  Activity Report on Neutron Scattering Research: Experimental Reports **23** (2017) Report Number: 1813

- Switching the magnetic order in CaBaCo2Fe2O7 using magnetic field
  J. Reim, M. Valldor, W. Schweika, T. J. Sato
  Activity Report on Neutron Scattering Research: Experimental Reports **23** (2017) Report Number: 1826

- Study of the Magnetic Structure of the Noncentrosymmetric Heavy-Electron Metamagnet CePdSi3 under Magnetic Fields
  M. Yoshida, D. Ueta, T. Kobuke, Y. Ikeda, H. Yoshizawa
  Activity Report on Neutron Scattering Research: Experimental Reports **23** (2017) Report Number: 1834

- Study of the Magnetic Structure of the Noncentrosymmetric Heavy-Electron Metamagnet CePtSi3
  M. Yoshida, D. Ueta, T. Kobuke, Y. Ikeda, H. Yoshizawa
  Activity Report on Neutron Scattering Research: Experimental Reports **23** (2017) Report Number: 1835

- Magnetic structure of pressure-induced ordered state in CsFeCl3
  Shohei Hayashida and Takatsugu Masuda
  Activity Report on Neutron Scattering Research: Experimental Reports **23** (2017) Report Number: 1838

- Electrical control of magnetic moment on multiferroics Ba2MnGe2O7
  S. Hasegawa, S.Hayashida, R. Sibille, T. Masuda
  Activity Report on Neutron Scattering Research: Experimental Reports **23** (2017) Report Number: 1847

- Magnetic structure of Weyl semimetal candidate NdGaSi
  Minoru Soda
  Activity Report on Neutron Scattering Research: Experimental Reports **23** (2017) Report Number: 1848

- Neutron diffraction study on magnetic structure in CaCoV2O7
  R. Murasaki, K. Nawa, M. Avdeev and T. J. Sato
  Activity Report on Neutron Scattering Research: Experimental Reports **23** (2017) Report Number: 1852

- Detection of magnetic scattering of Zn-Nd-Zn single ion magnet using xyz polarization analysis
  Maiko Kofu, Takashi Kajiwara, Michihiro Nagao, Osamu Yamamuro
  Activity Report on Neutron Scattering Research: Experimental Reports **23** (2017) Report Number: 1853

- Magnetic Order of magnetoplumbity-type cobalt oxide SrCo12O19
  Asai S., Kikuchi H., and Masuda T.
  Activity Report on Neutron Scattering Research: Experimental Reports **23** (2017) Report Number: 1856

- Current driven motion of skyrmions in MnSi
  D. Okuyama, M. Bleuel, Q. Ye, P. D. Butler, A. Kikkawa, Y. Taguchi, Y. Tokura, D. Higashi, J. D. Reim, Y. Nambu, and T. J. Sato
  Activity Report on Neutron Scattering Research: Experimental Reports **23** (2017) Report Number: 1858

- Magnetic phase transition and magnetic structure on chiral magnetic Pr5Ru3Al2
  D. Okuyama, J. D. Reim, K. Makino, N. Booth, E. P. Gilbert, and T. J. Sato
  Activity Report on Neutron Scattering Research: Experimental Reports **23** (2017) Report Number: 1859

- Antiferromagnetic order in the Au-Al-Tb quasicrystalline approximant
  Sato T. J., Avdeev M., Ishikawa A., Sakurai A., Tamura R.
  Activity Report on Neutron Scattering Research: Experimental Reports **23** (2017) Report Number: 1874

- Short-range correlations in the new quantum kagome-lattice compound rm Yb_3Ni11Ge_4
  M. Takahashi, K. Nawa, M. Frontzek and T. J Sato
  Activity Report on Neutron Scattering Research: Experimental Reports **23** (2017) Report Number: 1878

- Magnetic Excitation of S=1/2 Breathing Pyrochlore compound Ba3Yb2Zn5O11
  Tendai Haku and Takatsugu Masuda
  Activity Report on Neutron Scattering Research: Experimental Reports **23** (2017) Report Number: 1880

- Novel magnetic state in a series of new square-lattice magnets
  Tendai Haku and Takatsugu Masuda
  Activity Report on Neutron Scattering Research: Experimental Reports **23** (2017) Report Number: 1881

Strongly Correlated Electron Systems

- Detecting quantum critical fluctuations in the distorted kagome Kondo compound CeRhSn
  Takahashi M., Adroja D. T., Demmel F., Yang C. L., Kim M. S., Takabatake T., Sato T. J.
  Activity Report on Neutron Scattering Research: Experimental Reports **23** (2017) Report Number: 1814

- Field-induced magnetic correlations in chiral lattice semimetals Ce3Co4Sn13 and Ce3Rh4Sn13
  K. Iwasa, Y. Otomo, K. Suyama, A. Goukasov, B. Gillon, J.-M. Mignot
  Activity Report on Neutron Scattering Research: Experimental Reports **23** (2017) Report Number: 1818

- Topological superconductor beta-PdBi2
  H. Furukawa, N. Kagamida, M. Soda
  Activity Report on Neutron Scattering Research: Experimental Reports **23** (2017) Report Number: 1833

- Magnetic-field dependence of spin correlation in chiral lattice semimetal Ce3Co4Sn13
  K. Iwasa, Y. Otomo, and J.-M. Mignot
  Activity Report on Neutron Scattering Research: Experimental Reports **23** (2017) Report Number: 1836

- Determination of the magnetic structure in weak ferromagnetic superconductor Tb0.47Y0.53Ni2B2C
  M. Takahashi and H. Furukawa
  Activity Report on Neutron Scattering Research: Experimental Reports **23** (2017) Report Number: 1863

- Neutron spin echo study on the iron-based ladder compound BaFe2S3
  Y. Nambu, M. Nagao
  Activity Report on Neutron Scattering Research: Experimental Reports **23** (2017) Report Number: 1871

- Search for magnetic reflection in CeRhSn under uniaxial pressure
  M. Takahashi, D. Okuyama, J. Fernandez-Baca, A. Aczel, T. Hong, C. L. Yang, M. S. Kim, T. Takabatake and T. J. Sato
  Activity Report on Neutron Scattering Research: Experimental Reports **23** (2017) Report Number: 1875

Glasses and Liquids

- Dynamics of super-high entropy liquids alkylated tetraphenylporphyrins
  O. Yamamuro, M. Nirei, M. Kofu, T. Nakanishi, G. Avijit, M. Tyagi
  Activity Report on Neutron Scattering Research: Experimental Reports **23** (2017) Report Number: 1867

- Fast Dynamics of Alkylammonium-based Ionic Liquids with Plastic-crystalline Phases
  O. Yamamuro, M. Nirei, M. Kofu, T. Yamada, M. Matsuki, M. Tyagi
  Activity Report on Neutron Scattering Research: Experimental Reports **23** (2017) Report Number: 1868

- Dynamics of K+ aqueous solution confined in [CuZn(CN)4]- host
  O. Yamamuro, M. Nirei, S. Nishikiori, M. Kofu, T. Kikuchi, W. Lohstroh
  Activity Report on Neutron Scattering Research: Experimental Reports **23** (2017) Report Number: 1869

Biology

- ATP-dependent functional domain motion of multi-domain protein MurD
  Hiroshi Nakagawa, Michihiro Nagao, Tomohide Saio
  Activity Report on Neutron Scattering Research: Experimental Reports **23** (2017) Report Number: 1816

- Subunit dynamics of alpha-crystallin under crowding condition
  Rintaro Inoue and Masaaki Sugiyama
  Activity Report on Neutron Scattering Research: Experimental Reports **23** (2017) Report Number: 1820

Soft Matters

- Quantitative evaluation of uniformity of various polymer networks by small angle neutron scattering (SANS) with contrast variation technique
  Nobuyuki Watanabe, Ken Morishima, Xiang LI, and Mitsuhiro Shibayama
  Activity Report on Neutron Scattering Research: Experimental Reports **23** (2017) Report Number: 1822

- Structural characterization of DNA-module gel by SANS
  Yusuke Yoshikawa, Xiang Li, Yui Tsuji, Mitsuhiro Shibayama
  Activity Report on Neutron Scattering Research: Experimental Reports **23** (2017) Report Number: 1827

- Structural analysis of conversion-limited critical cluster gel by small angle neutron scattering.
  Takako Noritomi, Kazu Hirosawa, Xiang Li, Mitsuhiro Shibayama
  Activity Report on Neutron Scattering Research: Experimental Reports **23** (2017) Report Number: 1831

- Effect of variety of alkanes on uidity and inter-lea et coupling of lipid membranes
  Hatsuho Usuda, Mafumi Hishida, Elizabeth Kelley, Michihiro Nagao
  Activity Report on Neutron Scattering Research: Experimental Reports **23** (2017) Report Number: 1844

- Elucidation of the Mechanism of the Solvent-Dependent Switch of Helical Main-Chain Chirality of Poly(quinoxaline-2,3-diyl)s in Alkanes by Small Angle Neutron Scattering
  Yuuya Nagata, Rintaro Inoue, Sota Sato, Kathleen Wood, Masaaki Sugiyama
  Activity Report on Neutron Scattering Research: Experimental Reports **23** (2017) Report Number: 1861

- Visualizing the correlation between branching point of homogeneous polymer gels
  Yui Tsuji, Xiang Li, and Mitsuhiro Shibayama
  Activity Report on Neutron Scattering Research: Experimental Reports **23** (2017) Report Number: 1862

- Structure analysis of metal-storing atom-mimicking dendrimers
  Takako Noritomi, Xiang Li, Ken Minagawa, Ken Albrecht, Kimihisa Yamamoto, Mistuhiro Shibayama
  Activity Report on Neutron Scattering Research: Experimental Reports **23** (2017) Report Number: 1870

Structures and Excitations

Crystal structure analysis of high temperature neutron diffraction data of novel oxide-ion conductor SrYbInO4

Kotaro Fujii, Ayaka Fujimoto, Masatomo Yashima
Tokyo Institute of Technology

Oxide-ion conductors, which include pure ionic conductors and mixed oxide-ion and electronic conductors, attract significant interest because of their varied uses in oxygen separation membranes and cathodes for solid-oxide fuel cells (SOFCs). The oxide-ion conductivity is strongly dependent on the crystal structure. At present, several structures, such as fluorites, perovskites, K_2NiF_4, mellilites, and apatites, are known to show high oxide-ion conductivities. For further development of oxide-ion conductors is investigating materials with new types of structures. According to such background, we are exploring new structure family of oxide-ion conductors. For example, we have discovered a new structural family of oxide-ion conductor $BaNdInO_4$ which has a monoclinic $P2_1/c$ perovskite-related phase with a layered structure, in 2014. More recently, we found novel material, $SrRInO_4$ (R : rare earths) with $CaFe_2O_4$-type structure showed high oxide-ion conductivity compared to the other $CaFe_2O_4$-type materials. In order to understand the mechanism of oxide-ion conduction, it is necessary to precisely determine the crystal structure (particularly position, occupancy factor, and anisotropic displacement parameters of oxygens) at high-temperature because oxide-ion conductors are generally used at high-temperature. In the present study, we investigated the crystal structure of $SrYbInO_4$ at high temperature using high resolution neutron powder diffractometer Echidna installed at the research reactor OPAL, ACNS, ANSTO. The material was prepared by the solid-state reaction. A pure oxide-ion conduction was observed at 1000 °C for $SrYbInO_4$ by electrical conductivity measurements. For the neutron diffraction experiments, the sintered pellets of the reaction products were introduced into a vanadium can and used for the neutron diffraction experiment. The measurements were carried out from room temperature to high temperature (1000 °C) at 200 °C intervals. Each measurement time was few hours. The structural analyses for these data are carried out by Rietveld method using the program RIETAN-FP. The Rietveld structure refinements of the diffraction data of $SrYbInO_4$ taken at the room temperature 23 °C, and 1000 °C using the orthorhombic *Pnma* $CaFe_2O_4$-type structure gave good quality of the fit and the reliability factors (R_{wp} =3.78 %, R_B = 3.82 % for 23 °C data, and R_{wp} = 3.33 %, R_B = 5.04 % for 1000 °C data). The unit-cell parameters and unit-cell volume V of $SrYbInO_4$ at 1000 °C (a = 10.0522(3) Å, b = 3.34702(9) Å, c = 11.7502(3) Å, V = 395.335(18) Å^3) are larger than those at RT (a = 9.920206(15) Å, b = 3.309496(4) Å, c = 11.636340(15) Å, V = 382.0313(9) Å^3), due to the thermal expansion. The bond lengths and equivalent isotropic atomic displacement parameters of $SrYbInO_4$ at 1000 °C are higher than those at RT, which indicates the larger thermal vibration at 1000 °C. The higher equivalent atomic displacement of oxygen atoms at 1000 °C suggests higher oxide-ion conductivity at 1000 °C compared to RT.

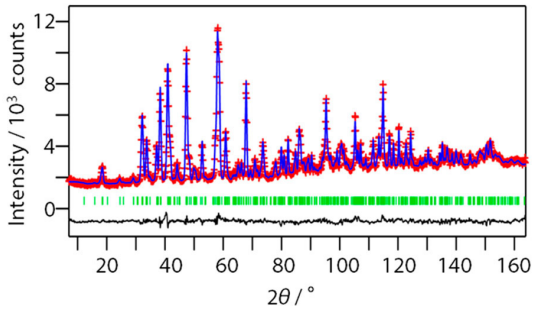

Fig. 1. Rietveld pattern of the neutron diffraction data of SrYbInO4 taken at 1273 K.

Magnetic structure of multiferroics $R\mathrm{Fe_3(BO_3)_4}$ (R =Ce, Sm)

Shohei Hayashida, Shunsuke Hasegawa, Shinichiro Asai, and Takatsugu Masuda
ISSP, University of Tokyo

Coexistence of magnetic order and electric polarization, *multiferroicity*, has become a top major topic over the past decade in condensed matter physics. In the multiferroic materials, rare-earth ferroborates $R\mathrm{Fe_3(BO_3)_4}$ (R = Y and rare-earth metal are a series of new multiferroic compounds containing the R^{3+} ($4f^n$) and Fe^{3+} ($3d^5$ $S = 5/2$) as magnetic ions [1]. The crystal structure is a trigonal and the space group is $R32$. The family of compounds shows diverse magnetoelectric (ME) effects as a function of the R^{3+} ions. In particular, the rare-earth ferroborates having the easy-plane type anisotropy exhibit huge ME effects. Thus we focus on $\mathrm{SmFe_3(BO_3)_4}$ and $\mathrm{CeFe_3(BO_3)_4}$ which have easy-plane type anisotropy. In $R\mathrm{Fe_3(BO_3)_4}$, the multiferroicity is explained by the spin-dependent metal-ligand hybridization mechanism, meaning that the local orientation of the magnetic moment plays a key role to determine the multiferroicity. It is important to identify the precise magnetic structure.

We performed neutron diffraction experiment to identify the magnetic structures of the $\mathrm{SmFe_3(BO_3)_4}$ and $\mathrm{CeFe_3(BO_3)_4}$. The single crystal samples were grown by a flux method. 99 % of the natural B and 98.9 % of the natural Sm were enriched by the ^{11}B and ^{154}Sm. The masses of the samples were 26 mg for $^{154}\mathrm{SmFe_3(^{11}BO_3)_4}$ and 23 mg for $\mathrm{CeFe_3(^{11}BO_3)_4}$. Neutron diffraction was performed by four-circle diffractometer HB-3A installed at ORNL. A vertically focusing silicon (022) monochromator was chosen to obtain the neutrons with the wave length of 1.542 Å. A closed cycle refrigerator was used to achieve 4.1 K as a base temperature.

The nuclear reflections measured at 4.1 K are reasonably refined by the trigonal structure with the space group $R32$ in both compounds, meaning that the symmetry of the crystal structure is retained at the low temperature.

Figure 1(a) shows the temperature evolution of the ω-scans of $^{154}\mathrm{SmFe_3(^{11}BO_3)_4}$ at $(-1, 0, 0.5)$. An additional peak appears below 33 K, and it is indexed by the propagation vector $\boldsymbol{k} = (0, 0, 1.5)$. This is consistent with the previous powder neutron diffraction measurement [2]. Unlike the $\mathrm{NdFe_3(BO_3)_4}$ [3], any incommensurate magnetic peak is not observed. Analysis of the magnetic peaks using Rietveld refinement, it is found that the magnetic moments of the Fe^{3+} ions form a collinear structure along the crystallographic a axis and they antiferromagnetically propagate along the c axis. The Sm^{3+} moment aligns in the ab plane but it is not parallel to the Fe^{3+} moments.

The temperature evolution of the l-scans of $\mathrm{CeFe_3(^{11}BO_3)_4}$ at $(-1, 0, 0.5)$ is shown in Fig. 1(b). Additional peaks appear around $l = 0.5$ below 30 K, meaning that a magnetic long-range order occurs at 30 K. This is consistent with the previous specific heat and magnetic susceptibility measurements of the polycrystalline sample [4]. The additional peak at $(-1, 0, 0.5)$ is indexed by the commensurate propagation vector $\boldsymbol{k} = (0, 0, 1.5)$, whereas the peaks at $(-1, 0, 0.45)$ and $(-1, 0, 0.55)$ are indexed by the incommensurate vector $\boldsymbol{k} = (0, 0, 1.5 + \delta)$ where $\delta = 0.042$ at 4.1 K. This incommensurability δ decreases with the increase of the temperature as shown in Fig. 1(b). From the measurement of the detailed temperature dependence of the l-scans, it is found that the transition temperature of the commensurate magnetic peaks differs from that of the incommensurate ones. This indicates that the phase separation between the commensurate and incommensurate magnetic structures occurs in the magnetic long-

range order. The detailed analysis of the magnetic structures in both compounds is now in progress.

References

[1] A. M. Kadomtseva *et al.*, Low Temp. Phys. **36**, 511 (2010).
[2] C. Ritter *et al.*, J. Phys.: Condens. Matter **24**, 386002 (2012).
[3] M. Janoshek *et al.*, Phys. Rev. B **81**, 094429 (2010).
[4] Y. Hinatsu *et al.*, J. Solid State Chem. **172**, 438 (2003).

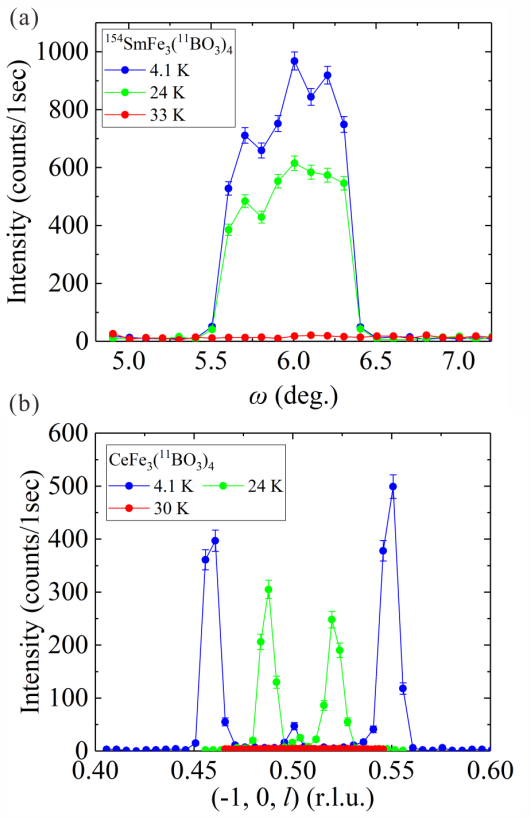

Fig. 1. (a) A temperature evolution of ω-scans of $^{154}SmFe_3(^{11}BO_3)_4$ at $(-1, 0, 0.5)$. (b) A temperature evolution of l-scans of $CeFe_3(^{11}BO_3)_4$ at $(-1, 0, 0.5)$.

Investigation of nano-precipitates in Ti-Al-Zr-Sn based alloy

Hiroaki MAMIYA
NIMS

Commercially titanium alloys are widely used for aircraft as a material having light weight (density being 60% that of steel), high strength, and excellent corrosion resistance. Many studies have been carried out to develop near-α titanium alloys for compressor discs and blades with improved tensile strength, fatigue resistance and creep performance at temperatures. However, it has been reported that solute partitioning in primary α grains causes formation of the α 2, Ti3(Al, Sn), phase. It is known that the low cycle fatigue resistance is reduced due to promotion of strain localization as a result of the presence of such α 2. This is a significant issue because the resulting lowered fatigue resistance can reduce the lifetime of compressor discs. IMI 834 is a typical near-α Ti-Al-Zr-Sn based alloy where small amounts of Si are added, consequently, the formation of fine ordered precipitates (Ti,Zr)6Si3 on the lamella boundaries improves the high-temperature strength. As stated here, the precipitates critically affect a combination of creep and low cycle fatigue properties, but the precipitation process is still not well understood. Hence, it is essential to clarify the nucleation and growth of the precipitates for further advances in aero-engines.

Our scanning and transmission electron microscopy (SEM, TEM), and three-dimensional atom probe tomography (3DAP) show small α 2 precipitates with size of a few nanometers in equiaxed alpha grains and slightly larger silicide precipitates with size of several tens nanometers on the lamella boundaries. However, SEM, TEM, and 3DAP are not suitable for detecting small variation in average size and in precipitate number density during heat treatments. For this reason, we measured small angle X-ray scattering but could not find any structures related to such precipitates in the obtained profiles. The reasons are that the scattering length density of α 2 for X-ray is similar to the matrix and that the scattering from the silicide exists outside the measuring range of our Lab-SAXS. For this reason, we measured wide q-range small angle neutron scattering using QUAKKA in ANSTO, to investigate mean size and number density of the nano-precipitates in variously aged IMI834, near-α Ti-Al-Zr-Sn based alloy.

The IMI 834 material has a composition of Ti-5.8Al-4.0Sn-80 3.5Zr-0.7Nb-0.5Mo-0.3Si-0.10O, in wt.%. The alloy was forged, then heat treated above the beta transus temperature. Finally, some were aged for various periods of 0, 10, 100, 200, or 400 hours at 650?C and of 0, 10, 100, 1300, or 2000 hours at 700 ?C. The samples are stable metal plates with thickness of approximately 0.5 mm. The measurements were performed in an atmospheric pressure at an ambient temperature using the sample autochanger. The observed q-range is from 6 x 10ˆ-3 ˆ-1 to 0.6 ˆ-1.

The obtained results are shown in Figure. We can find double shoulder-like anomalies on each profile for the samples with the aging treatments. The observations of SEM and TEM indicates that the anomaly in the low q region is caused by the precipitation of the silicide, while the anomaly in the higher q region is attributed to the α 2 precipitates. The positions of both the anomalies shift toward lower q with increasing the aging periods. This behavior is consistent with the results of microscopy. We are able to discuss their size distributions strictly when the compositions of these precipitates are determined by our on-going 3DAP measurements, then we can clarify nature of the precipitation in near-α titanium based alloy from differing points of view.

Uniaxial-stress-control of competing inter-chain exchange interactions of isosceles-triangular lattice Ising magnet CoNb2O6

Setsuo Mitsuda, Ryuta Henmi
Department of Physics, Faculty of Science, Tokyo University of Science

The isosceles triangular lattice Ising antiferromagnet is characterized by the ratio of exchange interactions defined as γ =J_1 (along the base direction) /J_2 (along the equilateral direction), and its magnetic property dramatically changes, depending on whether γ is larger than 1.0 or not. As one of the model materials, we have studied an Ising magnet $CoNb_2O_6$, where the quasi-1D ferromagnetic zigzag chains along the *c* axis form a frustrated antiferromagnetic isosceles-triangular lattice (ITL) with $\gamma \simeq 1.33$ in the *a*-*b* plane. If the exchange ratio γ can be controlled in $CoNb_2O_6$ via anisotropic deformation of ITL by uniaxial pressure, variety of interesting magnetic features intrinsic to γ would be observed.

Actually along this context, we succeeded in crossing the Wannier point (γ= 1) and providing access to the region of $\gamma < 1$ by further applying uniaxial pressure p up to 1GPa along the c axis, where AF-II magnetic ordering with q=1/2 is switched to AF-I magnetic ordering with q=0 at the critical pressure $p \simeq 0.8$GPa at which the exchange ratio γ becomes 1.0. This is what exactly suggested by Stephenson's exact calculation for 2D ITL, as is in the experimental reports 22 (N0 1802).

In present experiment, as a continuation of the proposal, we obtained entire $H_{//c} - T$ magnetic phase diagram (with γ∼0.91) at p= 1.1GPa, including determination of magnetic structure of magnetic state with q=1/5 newly appearing between AF-I magnetic ground state and field induced ferrimagnetic (FR) phase, as shown in Fig.1. How the IC phase appears in $H_{//c} - T$ magnetic phase diagram at p= 1.1GPa is entirely different from that at p= 0 Pa, corresponding to that one exchange J_1 (along the base direction) wins two exchange J_2 (along the equilateral direction) and there is essentially no competition among spins on isosceles triangular lattice for $\gamma < 1$. Level-crossing considerations using experimentally obtained four magnetic transition fields between AF-I, 5SL,FR,HHFR and IF phases as well as γ∼0.91 suggest that ten times smaller negative exchange J_4 and J_3'(compared with J_1 and J_2) is necessary for the appearance of 5SL and HHFR phases, respectively.

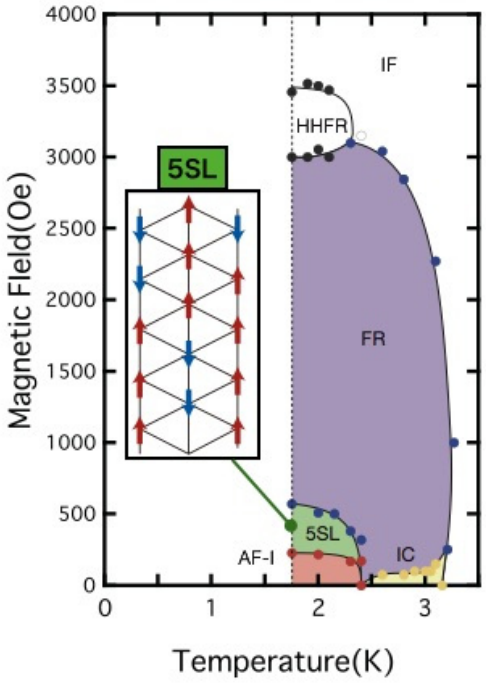

Fig. 1. H//c-T magnetic phase diagram at p= 1.1GPa.

Magnetic Ordering in S=1/2 Frustrated Square Lattice C20H19F6N5P

Minoru Soda
RIKEN Center for Emergent Matter Science (CEMS), Wako, Saitama 351-0198, Japan

Frustrated magnet has been extensively investigated both experimentally and theoretically. For quantum spins on the geometrical frustration systems, such as the pyrochlore, triangular, and kagome lattice systems, non-trivial ground states are expected. The simple quantum spin systems having one or two kinds of magnetic interactions have been reported in many solid materials while we can modify the magnetic interactions by using simple chemical modifications in organic radical compounds[1].

We focused on a verdazyl radical with delocalized pi-electron spins extending over the molecule, [o-MePy-V]+. The [o-MePy-V]+ molecule has a spin S=1/2 and forms the square lattice where six kinds of the magnetic interactions exist. From ab initio calculation, we can estimate the values of the magnetic interactions and found that the [o-MePy-V]+ square lattice has both ferromagnetic (F) and antiferromagnetic (AF) interactions. The [o-MePy-V]+ square lattice has the frustration induced by six kinds of the magnetic interactions, suggesting that exotic ground states are expected. In the specific heat measurement, the transition was observed at 1.8 K. However, the magnetic ground state in in C20H19F6N5P is not clear. Then, we try to clarify the magnetic structure of [o-MePy-V]PF6 (C20H19F6N5P) having the frustrated square lattice. The themes of (1) magnetism of pi-electron spin and (2) quantum spin in frustrated square lattice are very interesting,

We have carried out the neutron diffraction measurement in the single crystal C20H19F6N5P by using CORELLI (Elastic Diffuse Scattering Spectrometer) to examine the magnetic structure.

At 5 and 250 mK, the neutron intensities were measured in the wide Q-region. Figures 1 shows the neutron intensity measured at 250m K for Q=(H,K,H). The neutron intensities were observed at the fundamental Q-points. We examined the existence of the magnetic intensity by subtracting the neutron intensity at 5 K from that at 250 mK. As a result, we could not observe the obvious magnetic reflection. At this moment, we are trying the further analysis.

[1] H. Yamaguchi et al., PRB 88 174410 (2013).

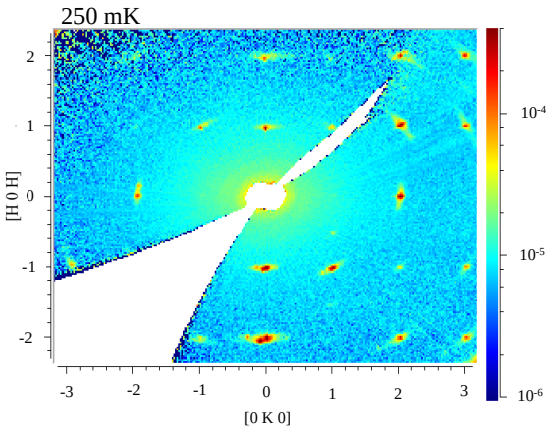

Fig. 1. Elastic neutron intensities measured at 250 mK for Q=(H,K,H).

Topological superconductor beta-PdBi2

Nao Kagamida
Ochanomizu University

In topological superconductors, it has been predicted that special particles, so-called Majorana fermions, will appear on the surface of the material. Recently, spin- and angle-resolved photoemission spectroscopy measurements revealed that Palladium-Bismuth Superconductor, β-PdBi2 (tetragonal structure, space group I4/mmm, Tc = 5.4 K[1]), has topologically protected surface state[2] and it attracts much attention.

In order to study bulk properties of PdBi2, we performed a small-angle neutron scattering (SANS) experiment and measured diffractions from vortex lattice. For the measurements, we grew single crystals of PdBi2 by a melt growth method and Tc of the crystals was evaluated to be Tc = 5.2 K by magnetization measurements. The previous neutron diffraction measurements at SANS-1 instrument in FRM-II (from 17th to 22th August, 2017) showed us clear spots. Q-dependence of the intensity indicates the system has hexagonal vortex lattice. Then, in the present study, to confirm the anisotropy and superconducting paring symmetry, we performed experiments at same instrument.

Four single crystals of PdBi2 (0.972 g, 0.856 g, 0.746 g and 0.506 g) were set with [010] axis vertical in a 3He insert, and it was installed into a magnet with horizontal fields. First, we checked positions of the crystals by neutron camera and set masks with Cd. After confirmation of a direction of field by using Nb single crystal, we measured vortex lattice created in field cooled process. A magnetic field was rotated from parallel to [001] towards [100] of the sample, in steps of α = 0, 15, 30, 45, 60, 67.5, 75, 82.5, 90 degree. Incident neutron beam was almost parallel to the magnetic field. We used neutrons with λ = 8 . Figures 1(a)˜(c) show diffraction patterns from vortex lattice at α = 0, 45 and 67.5 degree, respectively. Clear spots were observed. We determined a, b and anisotropy factor γ (= a / b) which were illustrated in Fig.1(a). We found that γ is highly dependent on α .
Next we measured temperature dependence of integrated intensity at H = 0.1 and 0.3 T by rotating the sample with the magnetic field around omega angle (around a vertical axis) at α = 0 degree. We will determine gap structure of this material.

This travel was done with a financial support by ISSP, University of Tokyo. We appreciate it pretty much since it could not be done without it.

References

[1] Y. Imai, F. Nabeshima, K. Miyatani, R. Kondo, S. Tsukada, & A. Maeda, J. Phys. Soc. Jpn. 81, 113708 (2012).
[2] M. Sakano, K. Okawa, M. Kanou, H. Sanjo, T. Okuda, T. Sasagawa & K. Ishizaka, Nature communications 6, 8595 (2015).

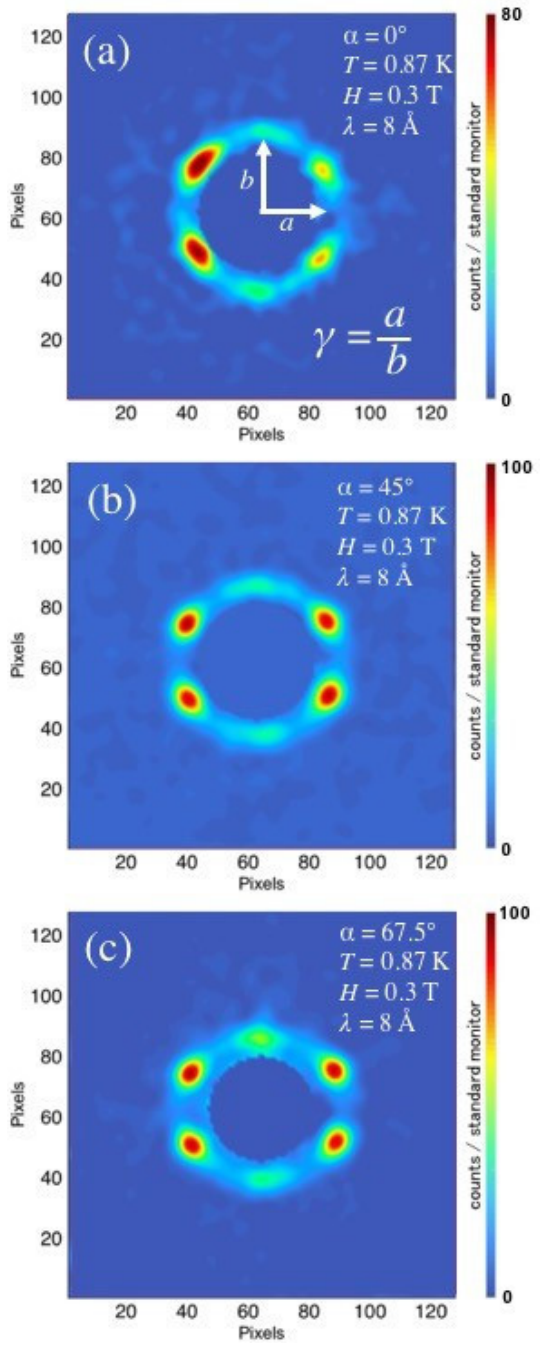

Fig. 1. Fig.1 SANS patterns at α = (a) 0 °(b) 45 °(c) 67.5 °at T = 0.87 K in H =0.3 T.

Structures and microscopic miscibility for nanoparticles of palladium-ruthenium-based alloys

O. Yamamuro(A), H. Akiba(A), K. Kusada(B), D. Wu(B), H. Kitagawa(B), D. Keen(C)
(A)ISSP-NSL Univ. Tokyo, (B)Kyoto Univ., (C)ISIS, RAL

Nanometer-size particles of alloys are attracting researchers in various scientific and industry fields. Recently we are focusing attention on PdRu alloys since they are expected to be high-performance and low-cost catalysts to remove CO and NOx in exhaust gas of cars. Pd and Ru atoms form bulk solid solutions only at much higher temperatures than room temperature (RT). This is mainly because Pd has an fcc structure while Ru has an hcp one. We have found that PdxRu1-x with a diameter of 5-7 nm are miscible in the whole composition range around RT [1]. However, the fcc and hcp phases coexist in a single nanoparticle. The present large problem is that the catalytic activity decreases due to the vaporization of Ru atoms at higher temperatures. In this study, we have performed the neutron powder diffraction (NPD) experiments on PdRuM (M = Rh, Pt, Ir) nanoparticles to investigate the miscibility improvement by adding the third metals M. The third metal may stabilize the alloys state due to the mixing entropy effect. These nanoparticles are covered with a protective polymer polyvinylpyrrolidone (PVP) to avoid adhesion between the nanoparticles. The NPD measurements were performed using the high-intensity neutron powder diffractometer (Polaris) installed at RAL, ISIS. NPD is powerful to distinguish between neighboring atoms in the periodic table such as Pd and Ru.

Figure 1 shows the atomic pair correlation function G(r) of Pd0.5Ru0.5 and Pd0.33Ru0.33M0.33 (M = Rh, Pt, Ir) nanoparticles obtained by the Fourier transform of the S(Q) data. The contribution from PVP has been subtracted. The red and green bars represent the positions and intensities calculated from the fcc and hcp structures. Both fcc and hcp peaks appeared in Pd0.5Ru0.5, Pd0.33Ru0.33Rh0.33 and Pd0.33Ru0.33Ir0.33, while only the fcc peaks in Pd0.33Ru0.33Pt0.33. This result demonstrates that adding Pt atoms is the most effective to stabilize the fcc structure and improve the miscibility of the alloy nanoparticles. Furthermore, we have found that the presence of much interface between fcc and hcp phases enhances the catalytic performance in PdRuM nanoparticles.

[1] K. Kusada et al., J. Am. Chem. Soc. 136, 1864 (2014).

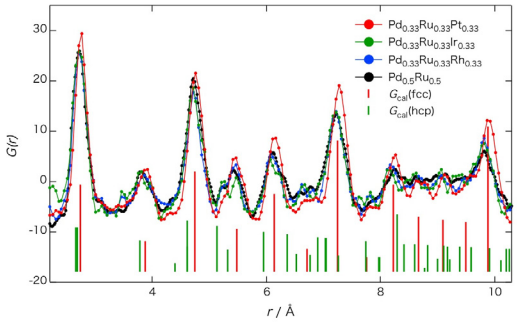

Fig. 1. Atomic pair correlation functions G(r) of Pd0.5Ru0.5 and Pd0.33Ru0.33M0.33 nanoparticles.

Magnetism

Magnetic diffuse scattering in pyrochlore antiferromagnet Na3Mn(CO3)2Cl

K. Nawa(A), D. Okuyama(A), M. Avdeev(B), and T. J. Sato(A)
(A)IMRAM, Tohoku Univ, (B)Bragg Institute, ANSTO

Spin systems with geometrical frustration have attracted much attention in the field of magnetism since they can exhibit unique magnetic structures, rich quantum phases, and critical phenomena. From this viewpoint, new compounds Na3T(CO3)2Cl (T = Mn, Co) should give an insight to approach the new quantum phases expected in pyrochlore antiferromagnets. This compound consists of TO_6 octahedra linked by carbonate ions (CO_3^{2-}), forming pyrochlore network of T^{2+} cations. For Na3Co(CO3)2Cl, previous macroscopic measurements and neutron scattering experiments [1] have revealed successive phase transitions in at T_a = 4.5 K and T_N = 1.5 K, described as a spin-glass like transition and all-in-all-out long-range magnetic order, respectively. However, the origin of the all-in-all-out magnetic order below the spin-glass temperature is still unknown. We believe that orbital degeneracy should be a key, since a coupling between the orbital degeneracy and a spin S = 3/2 for Co^{2+} (d^7) leads to a Kramers doublet of pseudo-spin 1/2 as a ground state. In fact, the temperature dependence of magnetic susceptibility is well reproduced by using high-temperature series expansions of spin 1/2 pyrocholore antiferromagnet.

To confirm our assumption, we prepared a new Mn-analogue, Na3Mn(CO3)2Cl. Its ground state should be different from Co-compound and may be intriguing because of the higher isotropy in magnetic interactions. In fact, the temperature dependence of magnetic susceptibility exhibits no clear anomaly down to 0.6 K, in contrast to Na3Co(CO3)2Cl. To investigate whether a magnetic order is present or not at low temperature, we performed neutron powder diffraction measurements using high-resolution powder diffraction spectrometer ECHIDNA at Bragg Institute, ANSTO. A dilution insert was used to reach down to 45 mK. Figure (a) shows diffraction patterns measured at 45 mK and 2.0 K, and difference of them. No additional magnetic Bragg peaks are present below 2.0 K, indicating the absence of a long-range magnetic order down to 45 mK. Instead, we find a diffuse scattering which develops below 50 K, as shown in Fig. (b). The bottom curve represents the intensity difference between 1.5 K and 200 K. A broad peak is clearly present at $Q \sim 0.85$ Å^{-1}, which is roughly close to $Q \sim 2\pi/d_{(110)}$ = 0.63 Å^{-1}, where $d_{(110)}$ = 10.04 Å corresponds to a doubled distance between nearest Mn-Mn atoms. This suggests that nearest neighbor antiferromagnetic correlations are dominant. Since the small difference in the spin correlations can be due to additional interactions such as dipolar-dipolar interactions, a further analysis for the diffuse scattering is necessary, which is in progress.

Our results reveal that Na3Mn(CO3)2Cl has a disordered ground state in contrast to Na3Co(CO3)2Cl which exhibits an all-in-all-out order. Since the former compound is a spin 5/2 system with isotropic magnetic interactions, the latter compound, which is pseudo spin 1/2 system, should have an anisotropy in magnetic interactions to exhibit the magnetic order. After analyzing the diffuse scattering patterns of Na3Mn(CO3)2Cl, reanalyzing those for Na3Co(CO3)2Cl using almost the same model except for single-ion and exchange anisotropy should reveal the origin of the unique magnetic transitions.

In summary, we conclude that a magnetic long-range order is absent down to 45 mK but antiferromagnetic short range order develops below 50 K for Na3Mn(CO3)2Cl. We are now analyz-

ing the diffuse scattering patterns to clarify magnetic interactions present in these unique pyrochlore compounds.

[1] Zhendong Fu et al., Phys. Rev. B, 87, 214406, (2013).

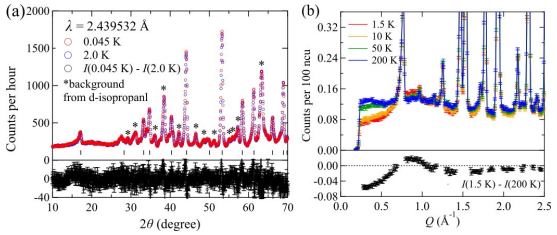

Fig. 1. (a) Neutron powder diffraction patterns measured at 0.045 K and 2.0 K. (b) Diffraction patterns measured at 1.5, 10, 50, and 200 K.

Switching the magnetic order in CaBaCo2Fe2O7 using magnetic field

J. Reim (A), M. Valldor (B), W. Schweika (C,D), T. J. Sato (A)
[A] *IMRAM, Tohoku University,* [B] *Max- Planck Institut, Dresden* [C] *JCNS, Forschungszentrum Juelich,* [D] *ESS ERIC*

The layered kagome system in the hexagonal Swedenborgite structure displays similarly to the Pyrochlores a highly frustrated network of tetrahedral coordinated magnetic ions. However, its broken inversion symmetry raises further the complexity of ordering due to non-vanishing Dzyaloshinski-Moriya (DM) interactions. The crystallographic structure of the compound $CaBaCo_2Fe_2O_7$ was successfully refined in $P6_3mc$ symmetry (a = 6.36 Å and c = 10.28 Å) and determined to be structural invariant under temperature within the resolution limits. Neutron scattering evidenced the coexistence of a seemingly commensurate K-type and long periodic (lp) modulation within the AFM phase (below 160 K). The latter one can be described with the 3-q star q_s^* of the propagation vector $q_s = (0.342, 0.342, 0)$ noted in the crystallographic unit cell. This corresponds to a splitting of $\delta \approx 0.017\,\text{Å}^{-1}$. Based on information from polarization analysis a spin structure was established using a model of superimposed cycloidal waves along each arm of the star q_s^*. The structure factor of the resulting spin structure corresponds semi-quantitatively with the observations. This model of the spin structure itself is an AFM skyrmion-lattice with a winding number of $w \approx -1$ indicating a topologically protected swirling.

In contrast to most ferromagnetic skyrmion-lattices, here no external magnetic field was applied to stabilize the long periodic modulation. This rises the question for the nature on the intrinsic stabilization mechanism. Magnetization measurements evidenced a non-vanishing field-hysteresis concluding a net magnetic moment at all measured temperatures (2 K up to room temperature). Depending on the sample's magnetic field history two different state exist (basically zero or non-vanishing net moment). In a more recent neutron scattering experiment, the intensity close to the K-point was discovered to be split, too, and corresponds to another lp modulation with a longer periodicity (inner $l_i \approx 1100$ Å and outer lp $l_o \approx 320$ Å). Furthermore, these two different lp modulations appeared to coexist in a wide temperature range within the AFM phase (cf. Fig. 1a). In correspondence with magnetization results, two states could be distinguished below 20 K: coexistence of two lp modulations (state A) or only the one with shorter periodicity remains (state B). Previous neutron scattering experiments hinted at the possibility to influence the magnetic order with an external field. In that experiment at the start the state A was observed, however applying an oscillating, decreasing magnetic field at room temperature led to a stabilization of state B. Yet, this change could not be reversed with magnetic fields up to 2 T.

The samples measured in the present experiment have been in state B at the start of the experiment, showing a coexistence at 80 K (see Fig. 1a) and a single lp modulation at 4 K (see Fig. 1b). The application of 5 T parallel and anti-parallel to the c-axis did not have any notable influence in the temperature range 4 to 80 K, however cooling in an applied field of 5 T from 160 K slightly changed the scattering pattern at low temperatures (see Fig. 1c). While, a complete switch to A could not be achieved, with the outer lp remaining dominant, this still underlines the possibility of a switch from state B to A.

Thanks to the improved resolution and decreased background, the two different modulations could be told apart clearly

and even the peak splitting of the inner modulation was resolved. Selected magnetic peaks have been measured at various temperature steps. From the 2D fits of these scattering maps we extracted not only the splitting magnitude but also the peak intensities of each individual peak. The resulting temperature dependence evidences the clear change of the dominant lp modulation for a sample in state B (see Fig. 1d). Since the inner lp modulation nearly vanishes at low temperatures, it can be hardly fit. Otherwise, both modulations' periodicity slightly increases with decreasing temperature, indicating both modulations to be incommensurate. Furthermore, for the first time an electric field of up to 0.5 kV/mm was applied along the high symmetry c-axis, however, at this field strength no change was observed in the scattering pattern.

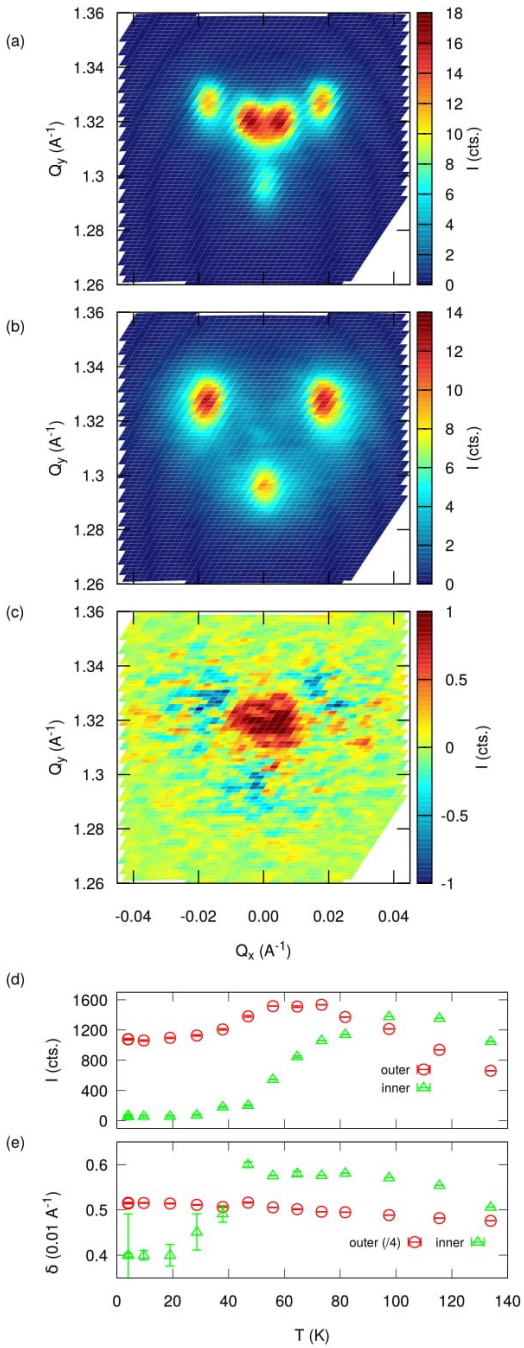

Fig. 1. Magnetic peak (2/3, 2/3, 0). (hk0)-scattering map at 80 K (a) and 4 K (b). (c) (hk0) map of the difference between measurements using FC and ZFC at 4 K. T dependence of the lp modulations' peak intensities (d) and splitting (e).

Study of the Magnetic Structure of the Noncentrosymmetric Heavy-Electron Metamagnet $CePdSi_3$ under Magnetic Fields

M. Yoshida[A], D. Ueta[A], T. Kobuke[A], Y. Ikeda[B], H. Yoshizawa[A]
[A]*ISSP-NSL, University of Tokyo,* [B]*IMR Tohoku University*

Noncentrosymmetric f-electron materials have attracted much attention because the absence of inversion symmetry leads to nontrivial and interesting effects upon physical properties. Recently, we have reported that the non-centrosymmetric $BaNiSn_3$-type compound $CePdSi_3$ exhibits successive magnetic transitions, multi-metamagnetic transitions, and weak ferromagnetism, yielding an unusually complex $H-T$ phase diagram [1]. We defined three phases as the Phase III, II and I as elevating temperature. From elastic neutron diffraction experiments at zero field performed in the last April, we found that magnetic peaks indicate a spin density wave (SDW) structure. In addition, the H and K domains coexist in $CePdSi_3$ at zero field.

In order to determine magnetic structures in $CePdSi_3$ under fields in the next step, we performed elastic neutron scattering experiments at BL-09 (CORELLI), SNS in Oak Ridge National Laboratory. A single crystalline sample of $CePdSi_3$ was grown by a flux method in the Institute for Solid State Physics. The sample was mounted on an Al pin such that both the a and c axes set into the equator plane and installed in SlimSam. Temperature was set to 1.9 K, and the magnetic-field was applied from 0 to 25 kOe along the H direction (the a axis).

We have succeeded in observing clear and interesting field dependence of the intensity of magnetic peaks as shown in Figure 1. The K domain disappears by 3 kOe, and only the H domain survives up to 12 ? 13 kOe where the phase changes I′ to IV. Surprisingly, in the field range from 10 to 15 kOe, our results indicate that a magnetic moment turns its direction perpendicular to the magnetic field with keeping the same modulation period. We have reported that a jump appears in the magnetization curve in the same field range [1]. Therefore, this behavior can be interpreted as a spin-flop transition. Finally, all magnetic superlattice peaks disappear above 20 kOe because of the forced ferromagnetism. We are in the middle of elucidation of a mechanism of such magnetic structures in field.

Travel expenses were supported by General User Program for Neutron Scattering Experiments, Institute for Solid State Physics, The University of Tokyo (proposal no. 17507), at JRR-3, Japan Atomic Energy Agency, Tokai, Japan.

Referenece

[1] D. Ueta *et al.*, J. Phys. Soc. Jpn., **85**, 104703 (2016).

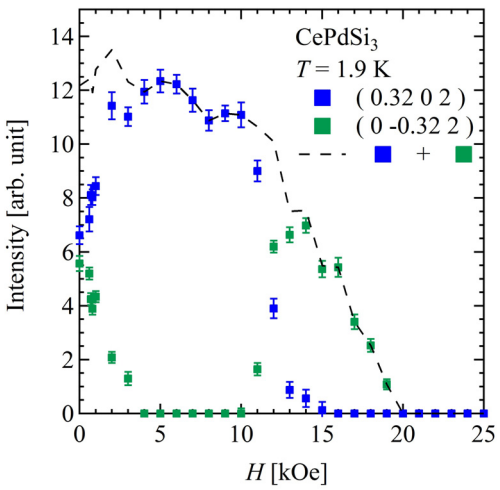

Fig. 1. Figure 1 The magnetic field dependence of the integrated intensity related to two propagation vectors in H- and K- domains. Blue and green indicate the H and K domains, respectively.

Study of the Magnetic Structure of the Noncentrosymmetric Heavy-Electron Metamagnet $CePtSi_3$

M. Yoshida[A], D. Ueta[A], T. Kobuke[A], Y. Ikeda[B], H. Yoshizawa[A]
[A]*ISSP-NSL, University of Tokyo,* [B]*IMR Tohoku University*

Noncentrosymmetric *f*-electron materials have attracted much attention because the absence of inversion symmetry leads to nontrivial and interesting effects upon physical properties. Recently, we have found that the non-centrosymmetric $BaNiSn_3$-type compound $CePtSi_3$ exhibits successive magnetic transitions, and multi-metamagnetic transitions in fields, yielding an unusually complex *H-T* phase, which is very similar to the *H-T* diagram of $CePdSi_3$ which we have recently reported [1]. We identified three phases at zero field and labeled them as Phase III, II and I as elevating the temperature. In order to determine magnetic structures for three phases at zero field in $CePtSi_3$, we performed elastic neutron scattering experiments at BL-09 (CORELLI), SNS in Oak Ridge National Laboratory. A single crystalline sample of $CePtSi_3$ was grown by a flux method in the Institute for Solid State Physics. The sample was mounted on an Al pin such that both the *a* and *c* axes set into the equator plane and installed in a Helium 3 insert. Temperature range was from 0.25 K to 5.5 K.

We found three magnetic peaks whose propagation vectors are $\tau_1 \sim (0, 0.27, 0)$, $\tau_2 \sim (0, 0.255, 0)$, and $\tau_3 \sim (0, 0.75, 0)$. The τ_1 peak was observed clearly in the Phase I and II, and disappears in the Phase III. On the other hand, the τ_2 and τ_3 peaks rapidly develop through the boundary between the Phase II and III. The temperature variations of the integrated intensity of these peaks are shown in Figure 1. Note that all the peaks vanish in the paramagnetic phase above 5 K, indicating that they are of magnetic origin. From these observation, we expect that two different spin density waves are formed depending on temperature.

Travel expenses were supported by General User Program for Neutron Scattering Experiments, Institute for Solid State Physics, The University of Tokyo (proposal no. 17904), at JRR-3, Japan Atomic Energy Agency, Tokai, Japan.

Reference

[1] D. Ueta *et al.*, J. Phys. Soc. Jpn., **85**, 104703 (2016).

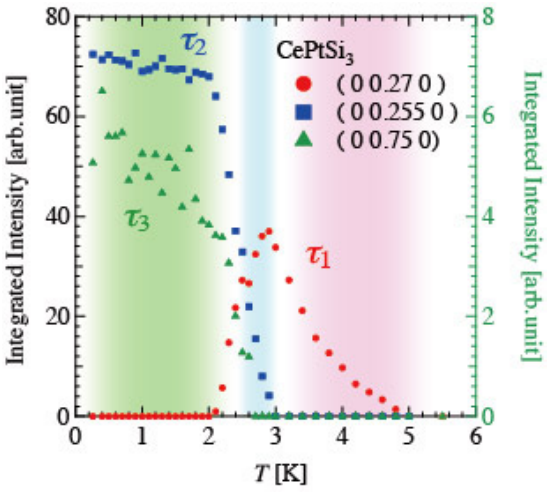

Fig. 1. Figure 1 The temperature dependence of the integrated intensity of three magnetic peaks. τ_1 : Circle(red), τ_2 : square (blue) and, τ_3 : triangle (green) indicate the propagation vectors related to these peaks.

Magnetic structure of pressure-induced ordered state in $CsFeCl_3$

Shohei Hayashida and Takatsugu Masuda
ISSP, University of Tokyo

$CsFeCl_3$ is an easy-plane type antiferromagnet having an integer spin. The crystal structure is a hexagonal with the space group $P6_3/mmc$. At ambient pressure and at zero magnetic field, a singlet ground sate is realized because of the strong easy-plane type single-ion anisotropy [1]. Recent magnetic susceptibility study demonstrated that applying pressure induces a magnetic long-range order [2]. Thus, $CsFeCl_3$ is an interesting compound exhibiting the pressure-induced quantum phase transition. In order to investigate the pressure-induced magnetic long-range order, we performed a single crystal neutron diffraction under pressures at ZEBRA diffractometer in Paul Scherrer Institut (PSI).

A single crystal sample was grown by the vertical Bridgman method. The single crystal was aligned so that the crystallographic *ab* plane was in the horizontal plane. We measured $(h\ k\ 0)$ and $(h\ k\ \pm 1)$ planes. The crystal was installed into the Hard Al-alloy piston cylinder pressure cell in PSI, and the cell was set in a ^{4}He cryostat. We used the tilting mode of 1D detector. Ge(311) monochromator was chosen to obtain the neutrons with the wavelength of 1.178 Å. A collimator of 80′ was installed between the sample and detector.

The pressures were estimated by measurement of the lattice constant of NaCl crystals mounted under the sample. We used the equations of state $V(P,T)$ for NaCl from Ref. [3]. The absolute accuracy of the pressure measurement was estimated to be ± 1 GPa. The obtained lattice constants of NaCl and calibrated pressures are shown in Table 1.

We observe additional peaks at $(h,k,0) \pm (1/3,1/3,0)$ by applying pressure $P = 0.9$ GPa. Figure 1 shows a temperature evolution of the intensity at $(1/3,1/3,0)$ and at $P = 1.8$ GPa. The intensity of the peak increases with decreasing temperature, meaning that it is a magnetic Bragg peak. From the indices of the magnetic peaks, it is found that a magnetic propagation vector $\boldsymbol{k}_{\rm mag}$ is $(1/3,1/3,0)$. The temperature evolution of the intensity was measured at several pressures. As a result, it is found that the transition temperature $T_{\rm N}$ increases with increasing the pressures as listed in Table 1.

In analysis of the magnetic structure, we use a representation analysis. The space group $P6_3/mmc$ and the magnetic propagation vector $\boldsymbol{k}_{\rm mag} = (1/3,1/3,0)$ lead to four irreducible representations (IRs) $\Gamma_3 + \Gamma_4 + \Gamma_5 + \Gamma_6$. The basis vectors for Γ_3 and Γ_4 provide an easy-axis type magnetic structure along the *c* axis, whereas those for Γ_5 and Γ_6 provide a coplanar 120° structure in the *ab* plane. As the result of the Rietveld refinement, we find that the magnetic structure for Γ_3 or Γ_6 is the answer. Since $CsFeCl_3$ has the strong easy-plane anisotropy, it is concluded that the structure for Γ_6 is the answer. Thus, the determined magnetic structure exhibits the 120° structure in the *ab* plane.

In summary, the single crystal neutron diffraction under pressure provided the evidence of the pressure-induced magnetic long-range order. Analyzing the magnetic reflections, the magnetic structure is the 120° structure with the propagation vector $\boldsymbol{k}_{\rm mag} = (1/3,1/3,0)$. In addition, the temperature evolutions of the intensities at several pressures shows the pressure dependence of the transition temperature.

References

[1] H. Yoshizawa *et al.*, J. Phys. Soc. Jpn. **49**, 144 (1980).
[2] N. Kurita and H. Tanaka, Phys. Rev. B **94**, 104409 (2016).
[3] J. M. Brown, J. Appl. Phys. **86**, 5801 (1999).

Table 1. Experimentally obtained lattice constant of NaCl and applied pressures at room temperature. Calibrated pressure referred by the table in Ref. [3].

NaCl lattice constant (Å)	Applied P (GPa)	Calibrated P (GPa)	T_N (K)
5.6948 (300 K)	0	-	-
5.5853 (1.6 K)	1.4	0.9	2.8
5.5588 (1.6 K)	1.6	1.3	3.8
5.5491 (1.6 K)	1.8	1.5	4.5
5.5351 (1.6 K)	2.2	1.8	5.5

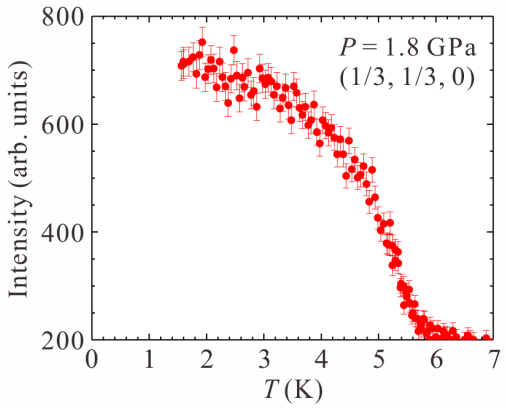

Fig. 1. A temperature evolution of the intensity at $(1/3, 1/3, 0)$ under $P = 1.8$ GPa.

Electrical control of magnetic moment on multiferroics $Ba_2MnGe_2O_7$

S. Hasegawa, S.Hayashida, R. Sibille, T. Masuda
ISSP, PSI

A multiferroic material $Ba_2MnGe_2O_7$ exhibits an easy-plane type antiferromagnetic order below $T_N = 4$ K [1], where the spin directs along crystallographic *a* axis and the antiferroelectric state is realized along the *c* axis. The electric polarization appears along *c* axis when magnetic field is applied along [110] direction [2]. Its multiferroicity is explained by the spin dependent $d-p$ hybridization mechanism. In this mechanism, since the local direction of the magnetic moment is related to the electric polarization, we can locally control the orientation of the magnetic moment by electric field. Although the study on the electrical control of the spin has been reported in an isostructural compound $Ba_2CoGe_2O_7$ [3], the magnetic moment has not been fully controlled from [100] to [110] directions because of its large magnetic anisotropy. In order to demonstrate the electrical control of the magnetic moment by the electric field in $Ba_2MnGe_2O_7$ having smaller anisotropy than $Ba_2CoGe_2O_7$7, we performed a single crystal neutron diffraction experiment under the electric field at ZEBRA diffractometer.

A single crystal sample was grown by the floating-zone method. The single crystal was aligned so that the crystallographic *ab* plane was in the horizontal plane. For the single crystal with a thickness of 0.85mm, aluminum electrodes were deposited onto the faces of (001) to apply the electric field. Maximum voltage in the used equipment was 5.0 kV. We measured $(h, k, 0)$-plane and $(h, k, 0.5)$-plane by using tilting mode in 1D detector. Ge311 monochromator was chosen to obtain the neutrons with the wavelength of 1.178A.

Magnetic Bragg peaks are observed below 4 K. From the analysis of the peaks, it is found that the easy-plane type antiferromagnetic structure having a magnetic propagation vector $\mathbf{k}_{mag} = (1, 0, 0.5)$ is realized, which is consistent with the previous research [1]. To investigate the electric field dependence, we performed the omega scan at (h, k, l)= (-3, -4, 0.5), (5, 0, 0.5) and its equivalent reflections. Figure 1 show electric field dependences of the omega scans at (h, k, l) = (-3, -4, 0.5), (3, -4, 0.5) and (5, 0, 0.5) at 2.9 K. The intensities at (-3, -4, 0.5) and (-4, -3, 0.5) increase with the increase of the electric field, whereas ones at (4, -3, 0.5) and (3, -4, 0.5) decrease. On the other hand, (5, 0, 0.5) and (0, -5, 0.5) are constant. In the analysis of the data, we assume that the magnetic moments continuously rotate from [100] (or [010]) to [110] directions when the antiferroelectric state becomes the ferroelectric state retaining antiferromagnetic structure by applying the electric field along the *c* axis. Under this assumption the intensity variation at (-3, -4, 0.5), (5, 0, 0.5) and its equivalent position is represented by the sinusoidal curve as follows:

$$I \propto 1 + \sin 2\theta \sin 2\omega$$

where I is the intensity of the each magnetic reflections, and the ω is a rotation angle of the magnetic moment from [100] or [010] to [110]. The θ is the angle between the scattering vector and *a* axis. The rotation angle of the magnetic moment is evaluated from the amplitude of the sinusoidal curve. From fitting the data, we obtained the rotation angle of magnetic moment against the electric field at several temperatures. Compared with the rotation angle at same temperature of 1.7K in $Ba_2CoGe_2O_7$, the one at 1.7 K in $Ba_2MnGe_2O_7$ is small. This is may be caused by the smaller electric polarization on $Ba_2MnGe_2O_7$ than that of $Ba_2CoGe_2O_7$. However, the rotation angle with temperature evolution is dramatically enhanced because the magnetic

anisotropy is strongly suppressed with the temperature evolution. The maximum rotation angle of spin direction is 21° at 2.9 K and at 5.9 MV/m. On the other hand, in over high temperature region, the rotation angle is likely saturated. Further analysis is needed to elucidate this behavior. In conclusion, the neutron diffraction experiment under electric fields has demonstrated the control of magnetic moment by electric field. In addition, the controllability is enhanced by the temperature evolution. In this experiment we achieve the maximum rotation angle of 21° at 2.9 K and at 5.9 MV/m.

References

[1] T. Masuda *et al.*, Phys. Rev. B **81**, 100402(R) (2010).
[2] H. Murakawa *et al.*, Phys.Rev. B **85**, 174106 (2012).
[3] M. Soda *et al.*, Phys.Rev. B **94**, 094418 (2016).

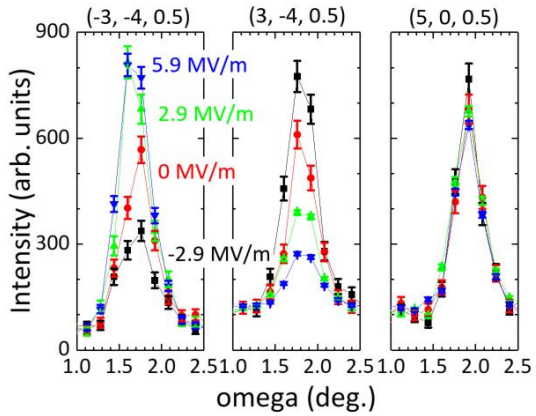

Fig. 1. The electric field dependences of the intensities at (-3, -4, 0.5), (3, -4, 0.5) at T =2.9 K.

Magnetic structure of Weyl semimetal candidate NdGaSi

Minoru Soda
IKEN Center for Emergent Matter Science (CEMS), Wako, Saitama 351-0198, Japan

Dirac and Weyl fermions have attracted great attention in condensed matter physics. In two dimensional graphene, massless Dirac fermions are realized, and the unique behaviour in the physical properties such as quantum Hall effect is observed. In three dimensional topological system, Weyl semimetal with an inversion symmetry-breaking is recently discovered for several semimetals. Weyl fermions induce the unique transport properties, such as the magneto-resistance induced by the chiral anomaly and the anomalous Hall effect. Then, the study of Weyl semimetal is very important for both foundation and application. On the other hand, the many reported Weyl semimetals with the polar structure have no magnetism. Although the relationship between the magnetism and the Weyl semimetal phase is discussed for several materials, such as Nd2Ir2O7, GdPtBi, and YbMnBi2, it is not clear.

We focus on the Weyl semimetal candidate having the magnetism, RGaSi (R=Pr, Nd, Gd, and Sm) [1]. In RGaSi, the crystal structure is classified by order/disorder of Ga/Si sites. The crystal structure with the order of Ga/Si sites belongs to the polar space group I41md same as the famous polar Weyl semimetal TaAs. Indeed, the realization of Weyl semimetal state has recently been suggested in the isostructural compound with the first principle calculation. Although many Weyl semimetals have the polar crystal structures, the relationship between the Weyl semimetal phase and the polar structure in RGaSi is not clear. Furthermore, RGaSi has the magnetism originated from the magnetic moment of R-ions, and the antiferromagnetic or ferrimagnetic transitions are observed at around 15 K. In the coexistence of the properties of the Weyl semimetal and the magnetism, the novel physical properties are expected. However, the magnetic structure of RGaSi is not clear. Then, we need to examine the magnetic ordering at low temperature. In order to clarify the relationship between the magnetic ordering and the physical property of Weyl semimetal, we carried out the magnetic structure analysis in Weyl semimetal NdGaSi.

We have carried out the neutron diffraction measurement in the single crystal NdGaSi by using HB-3A (Four Circle Diffractometer).

Figure 1 shows the temperature dependence of the integrated intensity at Q=(1,0,1). A small intensity at the Q=(1,0,1) exists above TN=12 K, which is originated from the nuclear reflection. With decreasing T, a large-intensity component due to magnetic ordering appears below TN. The magnetic diffraction measurements on the NdGaSi single crystal were carried out in order to clarify the magnetic structure. At 20 and 5 K, the neutron intensities were measured at many Q-points. The magnetic intensities were obtained by subtracting the integrated intensity at 20 K from that at 5 K. As a result, we observed the magnetic reflections at the fundamental Q-points. At this moment, we try to analyze the magnetic structure.

[1] G. Darone, et al., JSSC. 201, 191 (2013).

Neutron diffraction study on magnetic structure in CaCoV2O7

R. Murasaki (a), K. Nawa (a), M. Avdeev (b) and T. J. Sato (a)
(a) IMRAM, Tohoku University, (b) ANSTO

Among transition metal oxides, cobalt oxides provide a unique playground for the correlated electrons because of unquenched orbital angular momentum. In most cobalt oxides, a coupling between residual orbital degrees of freedom (L = 1, effectively) and spin S =3/2 is present, leading to an effective total angular momentum Jeff = 1/2. The collective magnetism of Jeff = 1/2 of the cobalt oxides can be interesting, since anisotropy of magnetic interactions between Co ions can be tuned by a distortion of the octahedra [1]. From this viewpoint, we have explored magnetism of cobalt oxides and found a cobalt oxide CaCoV2O7 [2]. This compound consists of two CoO6 octahedra which are crystallographically inequivalent. The two octahedra share their edge and form a dimer of Jeff = 1/2. Our preliminary magnetization measurements revealed possible complicated successive magnetic transitions at TN1 = 4 K and TN2 = 3.2 K. As the magnetic structure of the ordered phases are totally unknown, we performed neutron diffraction study.

The experiment was performed at ECHIDNA high-resolution neutron powder diffractometer of Australian Nuclear Science and Technology Organisation. The Ge 311 reflections were used for the monochromator to select neutrons with the wavelength 2.44 Ang. The powder samples were set in the 4He cryostat with the base temperature being 1.6 K. Diffraction patterns at several temperatures were measured between 1.6 K and 4.5 K to elucidate evolution of the magnetic structures in this temperature range.

As an representative result, Fig. 1 shows the neutron powder diffraction patterns measured at T = 1.6 K and 4.5 K. There are quite a few Nuclear Bragg reflections observed in the whole 2-theta range. Preliminary structural analysis confirms good quality of the sample used in the neutron diffraction study. At the base temperature T = 1.6 K, we can clearly see the development of the new peaks at low 2-theta region, indicating magnetic reflections appear below the magnetic ordering temperature. We are presently working on the analysis of the magnetic diffraction pattern using the representation analysis.

[1] M. E. Lines, Phys. Rev., 131, 546 (1963).
[2] E. V. Murashova et al., Zh. Neorg. Khim., 38, 1446 (1993).

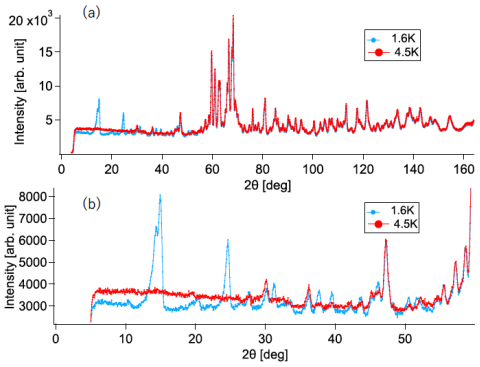

Fig. 1. (a) Neutron powder diffraction patterns measured at T = 4.5 K and 1.6 K using ECHIDNA high-resolution diffractometer at ANSTO. (b) Magnified plot for the lower 2-theta region.

Detection of magnetic scattering of Zn-Nd-Zn single ion magnet using xyz polarization analysis

Maiko Kofu[1], Takashi Kajiwara[2], Michihiro Nagao[3], Osamu Yamamuro[4]
[1]*J-PARC Center, JAEA,* [2]*Nara Women's University,* [3]*National Institute of Standards and Technology,* [4]*ISSP, University of Tokyo*

A single-molecule magnet (SMM) is a metal complex that behaves as an individual nanomagnet. Each molecule, containing several metal centers with unpaired electrons, possesses a giant resultant spin. Given that the giant spin exhibits easy-axis anisotropy ($D>0$), the magnetization reversal between the ground states with $J_z = \pm J$ is hindered by the potential barrier of DJ_z^2. The over-barrier activation is a diffusive process that requires the system to absorb phonon energy to be excited over the potential barrier. This is a spin-phonon relaxation mechanism (Orbach mechanism). Early SMM researches have focused on the complexes containing multiple transition metal ions. During the past decade, lanthanide SMMs have received much attention as promising materials with high blocking temperature, i.e. stable SMMs [1, 2]. Owing to a large contribution of angular momentum, lanthanide complexes can become SMMs containing only one or two magnetic ions. However, the relaxation behaviors of lanthanide SMMs are rather complicated and several types of mechanisms are discussed, for example Raman, direct and quantum tunneling processes. Clarifying the mechanism of magnetic relaxation is a key issue in lanthanide SMMs and assists formulation of designing strategies for engineering long-living SMMs.

We have previously studied a Tb-Cu dinuclear SMM by inelastic (INS) and quasielastic neutron scattering (QENS) [3, 4]. We are now investigating trinuclear Zn-Ln-Zn complexes (Ln = Ce, Pr, Nd) [5, 6]. The system has only one magnetic center in a molecule, in other words, which can be regarded as " single ion magnet ". Interestingly, the complexes with Kramers ion (Ce : $J = 5/2$ and Nd : $J = 9/2$) exhibit the superparamagnetic SMM behavior while that with non-Kramers ion (Pr : $J = 4$) does not [6].

We have made INS experiments on AMATERAS at J-PARC to search for magnetic excitations. There exists a strong magnetic excitation at 3-4 meV in the Pr complex but several weak excitations in a wide energy region (2 to 30 meV) in the Ce and Nd complexes. The feature of magentic excitations is closely related to whether it exhibits non-SMM or SMM behavior. QENS measurements were also made for the Nd complex using DNA and AMATERAS at J-PARC and a weak QENS contribution (about 1 % of elastic intensity) was observed. An overall dynamical map ranging from 1 ps to 10 ms, which is obtained by combining the QENS with ac susceptibility data, suggests that the magnetic relaxation does not simply follow the Arrhenius behavior. It indicates that the magnetic relaxation is not governed by the Orbach mechanism in this system.

However, one may consider that the relaxation observed in the QENS measurements is not from magnetic scattering of Nd but from incoherent/coherent scattering of other non-magnetic atoms. In fact, the complex contains many non-magnetic atoms (C, D, N, O, Zn···) and deuterium atoms can possibly move even below 100 K. In order to confirm that the relaxation observed in our QENS measurements is of magnetic origin, we have carried out an experiment with polarized neutron on NGA-NSE at NIST. Since there exist incoherent, coherent and magnetic scattering in Zn-Ln-Zn systems, a xyz polarization analysis is

necessary to extract the magnetic scattering component. The NGA-NSE spectrometer is suited to perform the xyz analysis, since it uses polarized neutrons and Q-coils.

Figure 1 shows the evaluated magnetic scattering in the temperature range from 3.5 K to 125 K. The fraction of magnetic scattering (f_{mag}) at 3.5 K is about 0.8 % which agrees with that of QENS contribution. The fraction gradually decreases upon heating due to the activation of magnetic relaxation and a decrease in population of ground state. We have also measured charcoal (non-magnetic) as a reference and its magnetic scattering is estimated to be 0 ± 0.2 % from the xyz analysis. Therefore we could argue that the relaxation detected in QENS is really magnetic.

We are now undertaking further analysis to probe the hybridization of ground state in the Nd SMM. Since the intensity of elastic magnetic scattering is proportional to J_z^2 of the ground state, the estimate of the intensity enables us to understand the degree of hybridization of states. Particularly, the comparison of the elastic intensity with the excitation ones (obtained in the INS measurements) is helpful to discuss a spin Hamiltonian. We consider that our comprehensive study using neutron scattering techniques can characterize the Zn-Ln-Zn complexes and understand the mechanism of magnetization reversal.

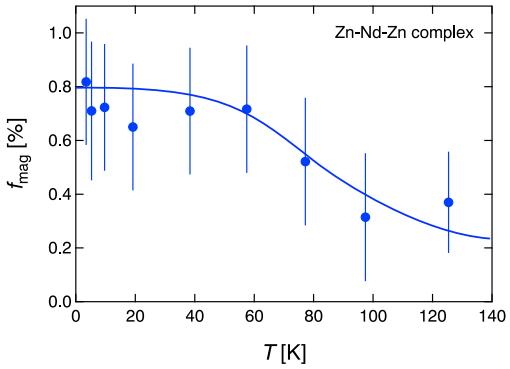

Fig. 1. Fraction of magnetic scattering as a function of temperature.

References

[1] R. Sessoli *et al.*, Coordin. Chem. Rev. **253**, 2328 (2013).

[2] D. N. Woodruff *et al.*, Chem. Rev. **113**, 5110 (2013).

[3] M. Kofu *et al.*, Phys. Rev. B **88**, 064405 (2013).

[4] M. Kofu *et al.*, Chem. Phys. **427**, 147 (2013).

[5] S. Hino *et al.*, Dalton Trans. **42**, 2683 (2013).

[6] C. Takehara *et al.*, Dalton Trans. **44**, 18276 (2015).

Magnetic Order of magnetoplumbity-type cobalt oxide $SrCo_{12}O_{19}$

Asai S., Kikuchi H., and Masuda T.
Institute for Solid State Physics, the University of Tokyo

Various physical properties of cobalt oxides has been intensively investigated, which comes from the variety of the electronic states for Co ions. 2+, 3+, and 4+ are stable for the valence of Co ions in oxides. Additionally, the Co^{3+} ions surrounded by oxygen ions octahedrally can take two different electronic configurations, high-spin state (S = 2) and low-spin state (S = 0). $SrCo_{12}O_{19}$ has the magnetoplumbite-type crystal structure as shown in Fig. 1(a) [1]. There are 5 equivalent sites for Co ions in the unit cell. From the bond-valence sum analysis, the valence of the Co ions in Co(3) and Co(4) sites is predicted to be 3+ and 2+, respectively [1]. On analogy of $SrCo_6O_{11}$ [2], the Ising-like character is expected for the spins of the Co(3) ions. The uniaxial colossal magnetoresistance was observed in the insulating phase [3]. Ishiwata *et al*. suggests that the origin of the magnetoresistance is that the charge order in the conduction paths, which is formed by the Co(1), Co(2), and Co(5) sites, is destabilized by the applied field [3]. The magnetic susceptibility has a sharp increase in the case that the magnetic field is perpendicular to the crystallographic c axis at 80 K [3]. It suggests the magnetic long-range order. The magnetic structure should be investigated to clarify the origin of the magnetoresistance. Neutron diffraction experiment was performed on High-Intensity Powder Diffractometer WONBAT installed at ANSTO. We used the orange cryostat for achieving low temperature. The PG filter is located in front of the sample. We used 0.9 g of the sample. We chose the neutron wavelength of 2.41 Å. Figure 1(b) shows the neutron diffraction patterns at 1.5 and 100 K. We observed the magnetic peaks indexed by (004), (101), (103), (006) or (104), and (105). It suggests that the magnetic propagation vector k_{mag} is (0, 0, 0). The temperature dependence of the integrated intensity for the magnetic (101) peak is shown in Fig. 1(c). The peak intensity gradually increases with increasing temperature below 80 K, which is the magnetic transition temperature determined by the magnetic susceptibility. It indicates that these magnetic peaks are intrinsic. The magnetic structure analysis is still in progress.

[1] S. Ishiwata *et al*., J. Solid State Chem. **181**, 1273 (2008). [2] S. Ishiwata *et al*., Phys. Rev. Lett. **98**, 217201 (2007). [3] S. Ishiwata *et al*., Phys. Rev. B **83**, 020401 (2011).

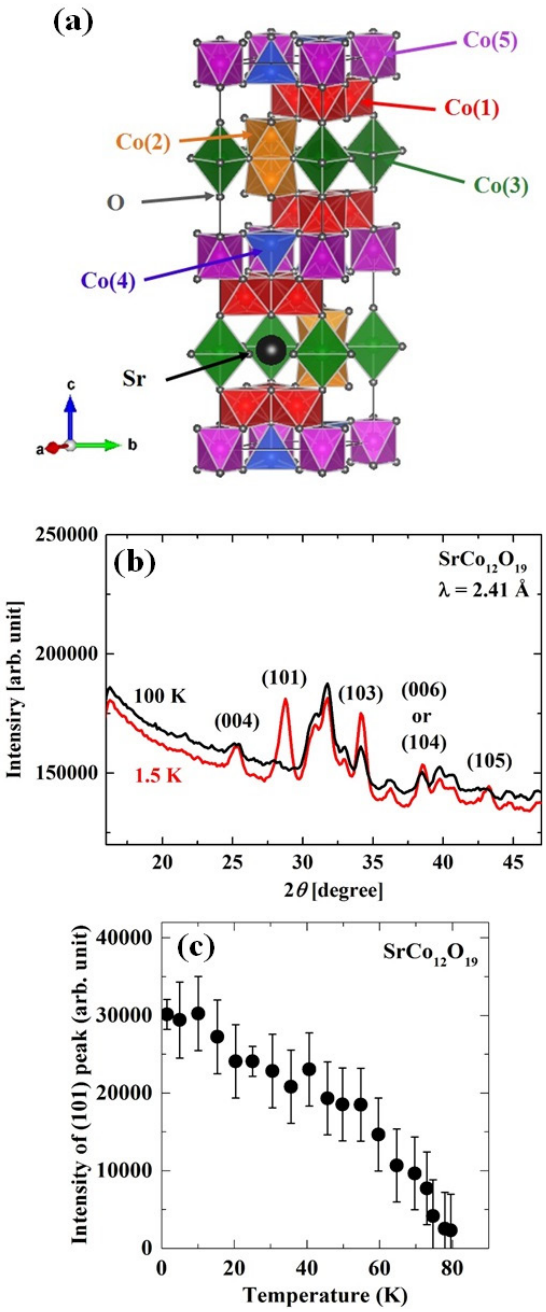

Fig. 1. (a) Crystal structure of $SrCo_{12}O_{19}$. (b) Neutron diffraction patterns at 1.5 and 150 K. (c) Temperature dependence of the integrated intensity for (101) magnetic peak.

Current driven motion of skyrmions in MnSi

D. Okuyama(A), M. Bleuel(B), Q. Ye(B), P. D. Butler(B), A. Kikkawa(C), Y. Taguchi(C), Y. Tokura(C,D), D. Higashi(A), J. D. Reim(A), Y. Nambu(E), and T. J. Sato(A)
(A)IMRAM, Tohoku Univ., (B)NCNR, NIST, (C)RIKEN-CEMS, (D)Univ. of Tokyo, (E)IMR, Tohoku Univ.

Emergent electromagnetic field out of a topological spin texture is a novel concept in condensed matter, and has been intensively studied recently [1]. The skyrmion, a nontrivial swirling spin structure carrying a topological quantum number, is an intriguing example of such spin texture[2]. Its finite scalar spin chirality $S_i \cdot (S_j \times S_k)$ generates fictitious magnetic field acting on the conduction elections, giving rise to the nontrivial topological Hall effect in electron transport phenomena [3]. Inversely, it can be expected that the skyrmion motion is driven by the current flow, resulting in deformation, rotation, and translation of the skyrmion lattice. Recently, indeed, this current-driven rotation of the skyrmion lattice is experimentally observed at very low current density of 1 MA/m^2 [4]. Although this first experiment is tricky, realized only under temperature gradient, such low current density threshold for the skyrmion motion attracts special attention, as it opens a new way to manipulate spin structures by ultra-low electric current, a key technology to realize spintronics.

To investigate the deformation of the magnetic skyrmion lattice under the electric current flow, we performed SANS experiment with suppressing the thermal gradient as much as experimentally achievable. SANS experiments were carried out at NG7 (National Institute of Standards and Technology). The single crystal MnSi samples were grown by the Czochralski method, and were cut in the rectangular shape. The incident neutron wave- length was selected using the velocity selector as λ_i = 6 Å. To further reduce the temperature inhomogeneity in the measured region only a small part of the sample was illuminated by using narrow beam. An electric current was applied along the [0 0 1] direction. For such a large electric current, due to the self heating the sample temperature slightly deviates from the sensor temperature. However, the maximum difference between the sensor and sample temperatures was 0.16 K at j = 2.7 MA/m^2. The temperature gradient along the current-flow direction was also estimated, and was confirmed to be less than 0.035 K/mm at the sample region investigated in the present study under the maximum current density 2.7 MA/m^2. This is at least one order of magnitude smaller than the earlier work [3]. The sample mount was attached to the sample stick, and was installed in the horizontal-field magnet with the magnetic field applied along [1 -1 0] parallel to the incident neutron beam.

The magnetic skyrmion reflections were observed at the two temperatures, T = 28.3 K and 28.6 K, respectively, under B = 0.2 T and j = 0 MA/m^2. The six-fold magnetic reflections characteristic to the skyrmion lattice were observed in a temperature range of approximately 28 K $< T <$ 29.2 K at B = 0.2 T. This observation is identical to those in the earlier works, and confirms the reproducibility of the present measurement. The integrated intensity shows its maximum at T = 28.6 K, and then decreases at lower temperatures. The SANS patterns were also obtained under the finite electric current flow j = 2.7 MA/m^2 at B = 0.2 T. By comparing to SANS data at j = 0, one can clearly see considerable broadening of the skyrmion-lattice peaks in the azimuthal direction. The peak broadening is apparently temperature dependent; the width is considerably larger at T = 28.3 K compared to that at T = 28.6 K. This result clearly indicates sig-

nificant deformation of the skyrmion lattice under large electric current.

In summary, we clearly observed that the skyrmion peaks in the SANS pattern significantly broaden for $j > j_t$ (threshold current density), indicating that the skyrmion lattice considerably deforms when the lattice starts to flow.

Reference:
[1] N. Nagaosa and Y. Tokura, Nat. Nanotechnol. 8, 899 (2013).
[2] S. Muhlbauer, B. Binz, F. Jonietz, C. Pfleiderer, A. Rosch, A. Neubauer, R. Georgii, and P. Boni, Science 323, 915 (2009).
[3] A. Neubauer, C. Pfleiderer, B. Binz, A. Rosch, R. Ritz, P.G. Niklowitz, and P. Boni, Phys. Rev. Lett. 102, 186602 (2009).
[4] F. Jonietz, S. Muhlbauer, C. Pfleiderer, A. Neubauer, W. Munzer, A. Bauer, T. Adams, R. Georgii, P. Boni, R. A. Duine, K. Everschor, M. Garst, and A. Rosch, Science 330, 1648 (2010).

Magnetic phase transition and magnetic structure on chiral magnetic Pr5Ru3Al2

D. Okuyama(A), J. D. Reim(A), K. Makino(A), N. Booth(B), E. P. Gilbert(A), and T. J. Sato(A)
(A)IMRAM, Tohoku Univ., (B)ANSTO

Non-centrosymmetric materials are of growing interest recently, because of the possibility for a number of novel phenomena, such as parity-mixed superconductivity in metallic systems, bulk Rashba spin splitting of electron bands in polar materials, and non-trivial spiral or helical spin structures in magnetic materials originating from asymmetric spin-spin interactions. Nonetheless, materials that realize such intriguing phenomena are quite limited, and hence, new non-centrosymmetric materials have been actively sought out recently.

$Pr_5Ru_3Al_2$ is one of such new non-centrosymmetric materials, first synthesized by Murashova et al. [1]. Their first report includes magnetization measurements down to T = 4.2 K; possible ferromagnetic order was suggested at $T \sim 24$ K. Recently, we have succeeded in improving sample quality of $Pr_5Ru_3Al_2$ by employing several different heat treatments [2]. By using such high-quality single-phased polycrystalline sample, we have revisited magnetic properties, in particular, at further lower temperatures below 4.2 K. We found an antiferromagnetic ordering was observed at $T \sim 4$ K in the magnetic susceptibility for $Pr_5Ru_3Al_2$. Interestingly, further phase transition was observed above the 1000 Oe magnetic field for Pr5Ru3Al2, suggesting a formation of a complex magnetic phase diagram. On the other hand, the ferromagnetic anomaly for $Pr_5Ru_3Al_2$ at $T \sim 24$ K in the earlier report was not detected in our high-purity sample, and hence is attributed to the impurity contamination. Powder neutron diffraction experiment in $Pr_5Ru_3Al_2$ has been already performed. The diffraction data measured below the magnetic transition temperature ~ 4 K shows additional satellite magnetic reflections with long-period incommensurately modulated structure as shown Fig. 1 (b). Magnetic structure for $Pr_5Ru_3Al_2$ in the zero magnetic field and in 1.5 K $< T <$4.2 K is helical structure [2].

To investigate the magnetic structure of the $Pr_5Ru_3Al_2$, we performed SANS experiment at QUOKKA (ANSTO). The single crystal $Pr_5Ru_3Al_2$ sample was grown by long-time-anneal method. The incident neutron wave-length was selected using the velocity selector as λ_i = 5 Å. The sample mount was attached to the sample stick, and was installed in the horizontal-field magnet with the magnetic field applied along [1 -1 0] parallel to the incident neutron beam. Figure 1 shows the magnetic phase diagram determined by the magnetization measurement and the obtained SANS pattern. We found four magnetic phases. In phase II, we found four hold reflections at (q q q), which is consistent with the result of the neutron powder diffraction data [2]. At phase III, the two hold SANS pattern with the propagation vector (q q 0) was observed. 10 % increase of the Q-length at the phase transition from Phase II to Phase III is observed. From these results, it is also expected that the magnetic structure is changed.

In summary, we performed SANS experiment using $Pr_5Ru_3Al_2$ single crystal. It is clarified that the chiral magnetic $Pr_5Ru_3Al_2$ exhibits the complicated magnetic-field-induced phase transition. In phase II, the helical magnetic structure with incommensurate modulation was concluded. In contrast, in phase III, the different-type antiferromagnetic orderings with long-period incommensurately modulation vector takes place.

Reference:

[1] E.V.Murashova et al., Materials Re-

search Bulletin 45, 993 (2010).
[2] K. Makino, D. Okuyama, M. Avdeev, T.
J. Sato, J. Phys. Soc. Jpn. 85, 073705 (2016).

Antiferromagnetic order in the Au-Al-Tb quasicrystalline approximant

Sato T. J.(1), Avdeev M.(2), Ishikawa A.(3), Sakurai A.(3), Tamura R.(3)
(1) IMRAM Tohoku University, (2) ANSTO, (3) Tokyo University of Science

The Au-Al-Tb quasicrystalline approximant attracts growing attentions recently because of possible novel magnetic ordering inferred in the macroscopic measurements. This system has magnetic clusters consisting of nearly-icosahedrally arranged Tb magnetic moments, and thus is of considerable interest in its magnetic order. From the susceptibility measurements, a possibility for the antiferromangetic ordering has been proposed, however, no microscopic information on the magnetic ordering was obtained to date. We, hence, undertook the powder neutron diffraction experiment on the Au-Al-Tb approximant crystalline phase. The powder diffractometer ECHIDNA, installed at the OPAL reactor of ANSTO, was used, and the magnetic diffraction patterns in a wide temperature range from RT to 4 K were recorded.

As a result, we have clearly observed magnetic reflections below T $<$ 11 K. It may be noteworthy that the appearance of the magnetic peak perfectly coincides with the ordering temperature determined in the macroscopic susceptibility measurement. We found that the magnetic reflection was observed at Q = (1,1,1) position, indicating that the system undergoes antiferromagnetic transition with breaking bcc centering-translational symmetry. The 24 Tb-atom sites in the unit cell are all crystallographically equivalent, and hence we expect that the magnetic representation analysis would work well for the magnetic structure analysis of this kind. By using magnetic representation analysis, we found that the lowest temperature diffractogram is well reproduced by using two basis vectors belonging to one single irreducible representation. In real space, the basis vectors correspond to a noncollinear and noncoplanar spin structure defined on one single icosahedron, as shown in Fig. 1. The spins are found in the mirror plane of the Im-3 space group symmetry of the crystal, indicating that the local crystalline electric field effect plays deterministic role for the magnetic structure stabilization.

Further study on the magnetic symmetry and possible consequence of such nontrivial magnetic structure is in progress.

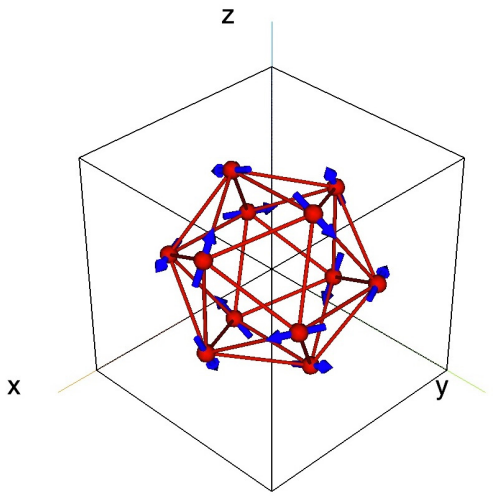

Fig. 1. Magnetic structure in one single Tb icosahedron determined in the present study. Note that the icosahedron on the vertex is depicted; the body-center icosahedron has antiparallel spin configuration.

Short-range correlations in the new quantum kagome-lattice compound $Yb_3Ni_{11}Ge_4$

M. Takahashi(A), K. Nawa(A), M. Frontzek(B) and T. J Sato(A)
IMRAM Tohoku University(A), ORNL(B)

Quest for quantum spin liquid state in two dimensional frustrated lattice has been at the heart of the condensed matter physics for decades. To detect such a exotic state, experimental research has been primarily conducted on insulating compounds where the quantum spin $S = 1/2$ is realized by the $3d^1$ or $3d^9$ state of the transition metal ions, such as Cu^{2+} or Ti^{3+}. Recently, Yb^{3+} based magnetic compounds attract growing attentions as a quantum frustrated system, because the ground-state Kramers doublets of Yb^{3+} may be regarded as pseudo spin $S = 1/2$.

In this work, we study the ternary intermetallic compound $Yb_3Ni_{11}Ge_4$, which has a breathing kagome-lattice structure where the quantum spin liquid state has been proposed theoretically[1]. First, we performed the magnetization and specific heat measurements. In both the experiments, anomaly due to a phase transition has not been observed down to 0.5 K. Instead, the C/T showed log-T increasing behavior below 2 K, and concomitantly magnetization curves indicated the development of in-plane antiferromagnetic correlations at low temperatures. To elucidate the log-T behavior and concomitant antiferromagnetic short range order, we performed powder neutron diffraction experiments using Wide-Angle Neutron Diffractometer (WAND) at ORNL. Neutrons with wavelength $\lambda = 1.488$ Å were selected by a monochromator using Ge 113 reflections. The powdered sample loaded in a copper can was set in the dilution refrigerator.

We measured powder diffraction patterns at the base temperature (∼50 mK) and two higher temperatures (0.8 and 4.5 K) between $2\theta = 1.4°$ and 122°. Figure 1 shows Q-dependence of the intensities at $T = 50$ mK and 0.8 K from which the high temperature (4.5 K) data were subtracted. Magnetic bragg peaks were not detected down to the lowest temperature. On the other hand, we can see the development of broad peaks due to antiferromagnetic short range order at the Q-position near 0 $Å^{-1}$ and 0.88 $Å^{-1}$, which correspond to the scattering vectors $Q = (0, 0, 0)$ and $Q = (1, 0, 0)$. It is likely that these fluctuations would be related to the $q = 0$ structure; the lattice in a crystal unit cell is divided into three sublattices where the direction of spins on one sublattice differs by 120° from that on other sublattices. The increase of intensity near $Q = (0, 0, 0)$ indicates the existence of ferromagnetic spin fluctuations. To detect the spin excitation spectra due to those spin fluctuations, and to confirm the exact Q-position of the diffuse scattering, we are planning to perform further neutron inelastic scattering experiment using a single crystal.

[1] R. Schaffer, Y. Huh, K. Hwang and Y. B. Kim, Phys. Rev. B 95, 054410 (2017).

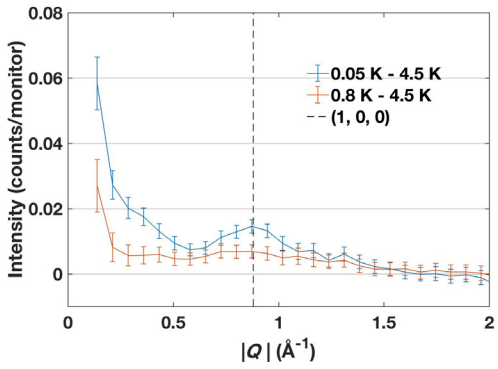

Fig. 1. Magnetic neutron-scattering patterns at $T = 50$ mK and 0.8 K obtained by subtracting a high temperature (4.5 K) data. The dashed line indicates the Q-position corresponding to the scattering vector $Q = (1, 0, 0)$.

Magnetic Excitation of S=1/2 Breathing Pyrochlore compound Ba3Yb2Zn5O11

Tendai Haku and Takatsugu Masuda
ISSP, the University of Tokyo

We studied low energy excitation in breathing pyrochlore compound Ba3Yb2Zn5O11 to identify the effective spin Hamiltonian using PELICAN spectrometer. The polycrystalline sample with the mass of 17.1 g was prepared by solid state reaction method. We used two setups for the inelastic neutron scattering (INS) experiment; setup I for high energy resolution using incident energy Ei of 2.1 meV, and setup II for coverage of wider Q - w space using Ei of 3.6 meV. Here Q is magnitude of scattering vector and w is energy transfer. Instrumental energy resolutions at the elastic position were 0.059 meV for setup I and 0.135 meV for setup II in full width at half maximum (FWHM). Closed cycle refrigerator was used to control the temperature T in the wide range, 1.5 K $<$ T $<$ 150 K.

Figures 1(a)-1(f) show INS spectra in the setup I measured at various temperatures. Three flat bands are observed at 1.5 K. The absence of dispersion suggests that these bands are approximately cluster excitations. The effect of the intercluster interaction is small and hidden in the instrumental resolution. At 6 K the intensities are suppressed and new flat bands appear at different ws. The intensities are small at 80 K, and the excitations are smeared out at 150 K. Several streaks observed in the range of w $<$ 0.4 meV in all the panels are acoustic phonons. Figures 1(g) and 1(h) shows the INS spectrum in the setup II.

One-dimensional energy cuts from the INS spectra in Figs. 1(a) and 1(c) are shown by symbols in Figs. 2(a) and 2(b), respectively. The peaks are fitted by Gaussian functions having FWHM of instrumental resolution to estimate the peak energies and the integrated intensities. The peak energies at 1.5 K are estimated as 0.39, 0.52, 0.73, 0.78 meV. At T = 12 K new peaks are observed at 0.21, 0.98, 1.03, 1.24, and 1.37 meV in Fig. 2(b). Temperature dependences of the intensities of the four peaks at 1.5 K are shown in Fig. 2(c), and those of the additionally observed peaks at 12 K are shown in Fig. 2(d). The formers monotonically decrease with the temperature and, in contrast, the latter increase with the temperature. This means that the probabilities of the initial states of the excitations observed at 1.5 K decrease with the increasing temperature and, therefore, the excitations are from the ground state and/or the excited state with small energy compared with 1.5 K. The additional excitations observed at 12 K are from the excited states.

Figure 2(e) shows one-dimensional energy cuts from the INS spectra at 1.5 K in Fig. 1(g) in setup II. A peak is observed at 1.75 meV in addition to the peaks observed in setup I. Q dependence of the intensity integrated in the range of 0.25 meV $<$ w $<$ 0.95 meV in Fig. 2(f) exhibits broad maximum at Qmax ˜ 1.25 -1. This means that antiferromagnetic correlation between the spins, the characteristic length scale of which is pi/ Qmax, is enhanced. The dispersionless excitations with the Q dependent intensity means that the neutron spectrum is dominated by an antiferromagnetic cluster within the instrumental resolution.

We analyzed the data on the basis of spin S=1/2 tetrahedron Hamiltonian including anisotropic and asymmetric interactions. The calculations are indicated by solid curves in Figs. 2(a)-2(f) and the data is reasonable reproduced. Detailed descriptions of the analysis and discussion are described in the paper [1].

[1] T. Haku, K. Kimura, Y. Matsumoto, M. Soda, M. Sera, D. Yu, R. A. Mole, T. Takeuchi, S. Nakatsuji, Y. Kono, T. Sakakibara, L.-J. Chang, and T. Masuda, Phys. Rev. B 93, 220407 (2016).

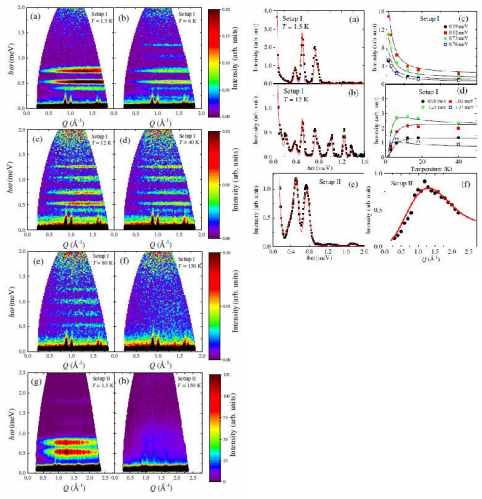

Fig. 1. Fig. 1 (right panel) INS spectra in false color map. Fig. 2 (left panel) 1D cut of INS spectra.

Novel magnetic state in a series of new square-lattice magnets

Tendai Haku and Takatsugu Masuda
ISSP, the University of Tokyo

Layered metal oxyfluorides/oxychlorides A2MO3X (A = Ca, Sr, M = Mn, Fe, Co, Ni, Cu, X=F, Cl) are members of a new family of 2D square lattice antiferromagnets [1,2]. In this study, we have paid attention to Sr2NiO3Cl and Sr2MnO3F. Neutron diffraction measurements on both samples were performed at a powder diffractometor Echidna in ANSTO. Although the ground state of Sr2MnO3F at 3 K is a conventional antiferromagnetic phase having q = (1/2, 1/2, 0), the magnitude of a magnetic moment was 3.04 μ B, which is suppressed from that of a free Mn3+ ion 4.0 μ B. The result suggests that magnetic fluctuation plays important role and disturb a magnetic order. We cannot understand the suppression with a simple 2D dimensionality. Hence we can expect that there are other type quantum fluctuations somewhere. On the other hand, we have not obtained experimental evidence for magnetic ordering on Sr2NiO3Cl by using a neutron diffraction technique.

We performed the powder inelastic neutron scattering on Sr2MnO3F and Sr2NiO3Cl at MERLIN in ISIS to reveal the magnetic excitation. On Sr2MnO3F, the measurements performed on a couple of temperature which is under and over the N el temperature. The Gd chopper was used and the speed was 400Hz. Ei were 50.1 meV, 26.2 meV and 16.0 meV. The measurement for Sr2NiO3Cl was performed under the N el temperature. We use the Gd chopper and the speed was 250Hz. Ei were 109 meV, 30 meV and 13.8 meV. The dispersion curve of which local minimum has at q = (1/2, 1/2, 0) and energy gap is 8 meV was observed. Since it is a typical behavior of a classical spin wave excitation of antiferromagnets with magnetic anisotropy, we are analyzing the data by the two-dimensional square lattice model with XXZ-type anisotropy. We cannot obtain any excitations on Sr2NiO3Cl. Combined with the diffraction data, Sr2NiO3Cl has no magnetic order or a magnetic order with a small ordered magnetic moment which cannot measure by using neutron scattering techniques. In any case, a magnetic order was disturbed by quantum fluctuations raised by both of low dimensionality and magnetic frustration.

[1] C. S. Knee et al., Phys. Rev. B 68, 174407 (2003).
[2] Y. Tsujimoto et al., Inorg. Chem. 51, 4802 (2012).

Strongly Correlated Electron System

Detecting quantum critical fluctuations in the distorted kagome Kondo compound CeRhSn

Takahashi M.(A), Adroja D. T.(B), Demmel F.(B), Yang C. L.(C), Kim M. S.(C), Takabatake T.(C), Sato T. J.(A)
IMRAM Tohoku University(A), ISIS (B), Hiroshima University(C)

Geometrically frustrated spin systems have been studied extensively for decades because of many intriguing phenomena, exemplified by the non-magnetic quantum disordered states. Also studied are non-magnetic ground states originating from Kondo-lattice-effect, such as those observed in Ce- and Yb-based intermetallic heavy-fermion compounds. Recently, a combination of the Kondo-effect and geometrical frustration becomes a new topic, both enhancing quantum fluctuations in different routes. This opens a new playground for the solid state physicists, and hence attracts special attention.

In this work, we study the heavy-fermion compound CeRhSn, which has a distorted kagome-lattice structure, a distorted version of a typical geometrically frustrated lattice. Recently, it has been reported that CeRhSn is indeed quite close to the quantum critical point, where divergence of quantum critical fluctuations were found below 1 K [1]. To elucidate the origin of this quantum critical behavior, we have performed neutron inelastic scattering experiment in this energy range (E $<$ 0.1 meV) using the backscattering spectrometer IRIS at ISIS. The experiment was performed using PG 002 reflections as analyzer, resulting in the energy resolution of 19 ueV at the elastic position. The sample was loaded in the dilution refrigerator with which the lowest attainable temperature was approximately 30 mK. To reduce the neutron absorption effect (of mainly Rh), the sample was cut in a thin plate shape.

We have measured the magnetic excitation spectra at the base temperature (˜ 30 mK) and high temperature (500 mK) on several representative loci in the Q-space. Fig. 1 shows the result at the base temperature on the Q-locus passing through Q = (1, 0, 0) and (1, 1, 0) at the elastic position. In addition to the single straight line observed at 0.25 meV, which is apparently the prompt pulse contamination, we see weak excitation intensity at 0.13 meV and Q ˜ (1, 0, 0). This inelastic intensity disappears at 500 mK, suggesting that it is indeed related to the quantum critical fluctuations. However, since the observed inelastic intensity is too weak to conclude its existence, we are planning to perform further experiments in future.

[1] Y. Tokiwa, C. Stingl, M.-S. Kim, T. Takabatake and P. Gegenwart, Sci. Adv. 2015;1 e1500001 (2015).

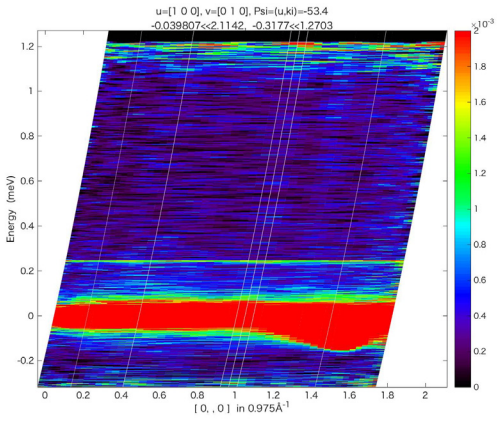

Fig. 1. Inelastic spectrum measured using the backscattering spectrometer IRIS at ISIS. The temperature was ˜ 30 mK. The locus at the elastic position was set to pass through both the Q = (1, 0, 0) and (1, 1, 0) positions.

Field-induced magnetic correlations in chiral lattice semimetals $Ce_3Co_4Sn_{13}$ and $Ce_3Rh_4Sn_{13}$

K. Iwasa[1], Y. Otomo[2], K. Suyama[2], A. Goukasov[3], B. Gillon[3], J.-M. Mignot[3]
Frontier Research Center for Applied Atomic Sciences, Ibaraki University, Japan[1]
Department of Physics, Tohoku University, Japan[2]
Laboratoire Léon Brillouin, CEA-CNRS, CEA/Saclay, France[3]

Electronic correlation phenomena have been central topics of solid-state physics. In the case of f-electron systems, the c–f hybridization effect has been a key issue. In addition, topological natures of electrons have recently been attractive recently: the electronic state of topological insulators of surface states and graphen are expressed as massless Dirac or Weyl fermions. A theoretical study have proposed a way to find three-dimensional (3D) bulk Weyl fermions in chiral symmetry lattices (J. L. Manñs, Phys. Rev. B **85**, 155118 (2012)). It is an attractive subject to find such chiral fermion systems and electronic correlations between the chiral fermions and the f electrons.

$Ce_3Co_4Sn_{13}$ has been reported to undergo a structural phase transition at 160 K (C. S. Lue et al., Phys. Rev. B 85, 205120 (2012)), and similar phenomena are also suggested for $Ce_3Rh_4Sn_{13}$ (A. Ślebarski et al., Phys. Rev. B **86**, 155122 (2012)). We evidenced low-temperature crystal structure categorized in the chiral space group $I2_13$ below the structural phase transitions at 160 and 352 K in $Ce_3Co_4Sn_{13}$ and $Ce_3Rh_4Sn_{13}$, respectively (Y. Otomo et al., Phys. Rev. B **94**, 075109 (2016)). The electrical resistivity data of $Ce_3Co_4Sn_{13}$ and $Ce_3Rh_4Sn_{13}$ are almost independent of temperature, in contrast to metallic behaviors of the La-based reference materials. These structural finding and transport property are expected to be signatures for the formation of Weyl semimetal state. The electronic Sommerfeld coefficients of these compounds reach approximately 4 J/(mol-Ce K^2) at 1 K (A. L. Cornelius et al., Physica B **378–380**, 113 (2006), A. Ślebarski et al., Phys. Rev. B **86**, 205113 (2012), E. L. Thomas et al., J. Solid State Chem. **179**, 1642 (2006)). This fact was understood as HF systems. However, our recent inelastic neutron scattering experiment revealed the emergence of spin excitations in the range up to 1 meV below 20 K (K. Iwasa et al., Phys. Rev. B **95**, 195156 (2017)), which originates from the crystal-electric-field (CEF) doublet ground state. Therefore, coherent spin dynamics emerge in the semimetal chiral phase. On the other hand, $Ce_3Co_4Sn_{13}$ and $Ce_3Rh_4Sn_{13}$ do not exhibit any magnetic ordering down to 0.5 K (K. Iwasa et al., in preparation), and previous study on $Ce_3Co_4Sn_{13}$ reported the field-induced antiferromagnetic correlations at 4.2 K (A. D. Christianson et al., Physica B **403**, 909 (2008)). Based on the $I2_13$ structure, the two inequivalent Wyckoff sites for the Ce ions take different CEF schemes (K. Iwasa et al., Phys. Rev. B **95**, 195156 (2017)). Thus, the magnetic-field-induced antiferromagnetic correlation can be understood different magnetic moments at the two Ce-ion sites. In order to examine such scenario for the Ce 4f-electron state, we performed polarized neutron diffraction measurements under the magnetic fields up to 6 T below 20 K, by using the hot-neutron diffractometer 5C1 installed in the Orphée reactor of Laboratoire Léon Brillouin.

Figure 1 shows measured intensity maps within the [1 0 0]-[0 1 0] reciprocal plane perpendicular to the applied magnetic fields of 6 T at measurement temperature of 2 K for $Ce_3Co_4Sn_{13}$. The measured results for the up (upper panel) and down (lower panel) spin polarizations of the incident neutron are not identical with each

other, in particular for the reciprocal-lattice region with h and $k < 10$. Similar polarization dependence was also observed for $Ce_3Rh_4Sn_{13}$. Such results indicate characteristic magnetic-moment distribution, the magnetic-scattering neutron wave from which interferes with the nuclear-scattering wave. Preliminary analysis for the flipping-ratio data shown in Fig. 1 based on the Cambridge crystallography subroutines give the magnetic moments of 1.5 and $0.9\mu_B$ at the two inequivalent Ce-ion sites. This result is consistent with the aforementioned structural and magnetic properties in the chiral phase.

We thank J.-L. Meuriot for technical support on performing the polarized neutron diffraction measurements. The experiments were supported by General User Program for Neutron Scattering Experiments, Institute for Solid State Physics, The University of Tokyo, at JRR-3, Japan Atomic Energy Agency, Tokai, Japan.

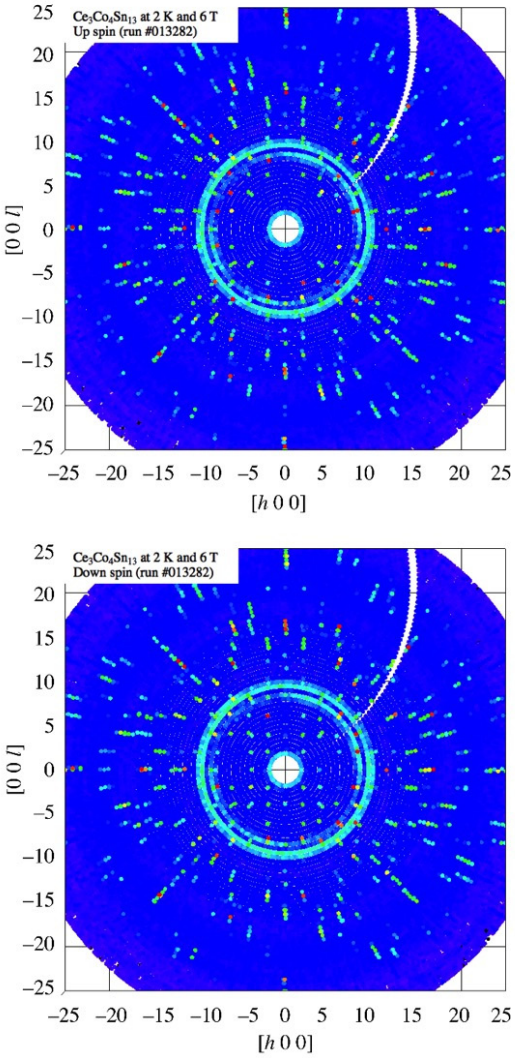

Fig. 1. Diffraction-intensity maps within the [100]-[010] reciprocal plane perpendicular to the applied magnetic fields of 6 T at measurement temperature of 2 K.

Topological superconductor beta-PdBi2

H. Furukawa(A)(B), N. Kagamida(A), M. Soda(B)
(A)Ochanomizu university, (B)RIKEN Institute, Japan

In topological superconductors, it has been predicted that special particles, so-called Majorana fermions, will appear on the surface of the material. Recently, spin- and angle-resolved photoemission spectroscopy measurements revealed that Palladium-Bismuth superconductor, β-PdBi2 (tetragonal structure, space group I4/mmm, Tc = 5.4 K [1]), has topologically protected surface state [2] and it attracts much attention.

In order to study bulk properties of PdBi2, including superconducting paring symmetry and other characteristic behavior of this material, we performed a small-angle neutron scattering (SANS) experiment and measured diffractions from vortex lattice. For the measurements, we grew single crystals of PdBi2 by a melt growth method and Tc of the crystals was evaluated to be Tc = 5.2 K by magnetization measurements. The experiment was carried out at the SANS-1 instrument in installed FRM-II from 17th to 22th Aug. 2017.

A single crystal of PdBi2 (0.75 g) was set with Nb (Fig.1) in a 3He insert with its cleavable c-plane vertical, and it was installed into a magnet with horizontal field. We first measured vortex lattice created in field cooled process. A magnetic field was applied parallel to the c-axis of the sample. Incident neutron beam was almost parallel to the magnetic field. Depending on the fields, we used neutrons with λ = 6, 8, 12 . Figures 2 (a) and (b) show typical diffraction patterns from vortex lattice. Clear spots were observed. Q-dependence of the intensity indicates the system has hexagonal vortex lattice.Next we measured temperature dependence of integrated intensity at H = 0.15, 0.2, 0.3, 0.4 and 0.45 T by rotating the sample with the magnetic field around phi angle (around a vertical axis).

This travel was done with a financial support by ISSP, University of Tokyo. We appreciate it pretty much since it could not be done without it.

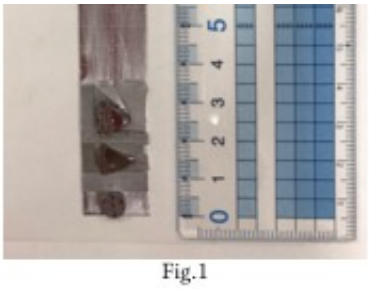

Fig.1

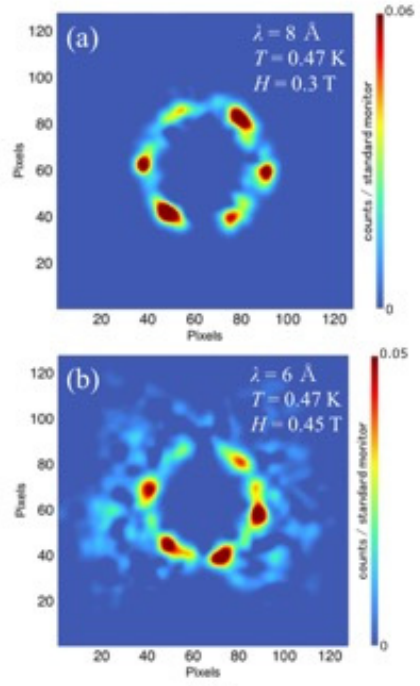

Fig.2

Fig. 1. Sample setting on an Al plate. From the top two single crystals of PdBi2 and one single crystal of Nb (bottom). Fig.2 SANS patterns at T = 0.47 K in (a) 0.3 T and (b) 0.45 T

Magnetic-field dependence of spin correlation in chiral lattice semimetal $Ce_3Co_4Sn_{13}$

K. Iwasa[1], Y. Otomo[2], and J.-M. Mignot[3]
Frontier Research Center for Applied Atomic Sciences, Ibaraki University, Japan[1]
Department of Physics, Tohoku University, Japan[2]
Laboratoire Léon Brillouin, CEA-CNRS, CEA/Saclay, France[3]

It is an attractive issue to investigate electronic correlation phenomena associated with topological symmetries. For example, massless Dirac/Weyl fermions have been extensively studied, which are characterized by linear dispersion for electron bands and have been identified for the two-dimensional systems. Recently, Dirac/Weyl electrons are also searched in three-dimensional (3D) bulk systems. It was discussed in a theoretical study that such 3D Weyl fermions intrinsically appear in chiral symmetry lattices [J. L. Manñs, Phys. Rev. B **85**, 155118 (2012)].

In the case of f-electron systems based on rare-earth alloy compounds, the c–f effect has been a key issue. Kondo semimetals or semiconductors exhibit band gap features as a consequence of such a hybridization effect. We expect that the Weyl fermions are formed in a Kondo semimetal taking a chiral symmetry structure. Considering such electronic state, we have investigated a class of $Ce_3Tr_4Sn_{13}$ (*Tr*: transition-metal elements).

$Ce_3Co_4Sn_{13}$ undergoes a structural phase transition at 160 K [C. S. Lue et al., Phys. Rev. B **85**, 205120 (2012)]. We evidenced that the low-temperature crystal structure takes the chiral space group $I2_13$ [Y. Otomo et al., Phys. Rev. B **94**, 075109 (2016)]. The electrical resistivity data of $Ce_3Co_4Sn_{13}$ is less dependent on temperature compared to metallic behaviors of $La_3Co_4Sn_{13}$ without $4f$ electrons. These facts are expected to indicate the formation of Weyl semimetal state in $Ce_3Co_4Sn_{13}$. The electronic Sommerfeld coefficients of these compounds was evaluated to be approximately 4 J/(mol-Ce K^2) at 1 K [A. L. Cornelius et al., Physica B **378–380**, 113 (2006), A. Ślebarski et al., Phys. Rev. B **86**, 205113 (2012), E. L. Thomas et al., J. Solid State Chem. **179**, 1642 (2006)]. This fact was understood as HF systems. However, our recent inelastic neutron scattering (INS) experiment revealed the emergence of spin excitations in the range up to 1 meV below 20 K [K. Iwasa et al., Phys. Rev. B **95**, 195156 (2017)]. On the other hand, $Ce_3Co_4Sn_{13}$ does not exhibit any magnetic ordering down to 0.5 K, and previous study on $Ce_3Co_4Sn_{13}$ reported the field-induced antiferromagnetic correlations at 4.2 K [A. D. Christianson et al., Physica B **403**, 909 (2008)]. Based on the $I2_13$ structure, the two inequivalent Wyckoff sites for the Ce ions take different CEF schemes [K. Iwasa et al., Phys. Rev. B **95**, 195156 (2017)]. Thus, the magnetic-field-induced antiferromagnetic correlation can be understood different magnetic moments at the two Ce-ion sites. In order to obtain microscopic information for the Ce $4f$-electron state, we performed INS measurements under the magnetic fields up to 6 T below 20 K, by using the cold-neutron spectrometer 4F2 installed in the Orphée reactor of Laboratoire Léon Brillouin.

Upper part of Fig. 1 shows INS spectra at the scattering vector $\mathbf{Q} = (1, 0, 0)$ for the original high-temperature unit cell of $Ce_3Co_4Sn_{13}$ measured at 1.6 and 20 K under magnetic fields of zero and 4 T applied along the $[0, -1, 1]$ axis. The data at 1.6 K and 4 T show a slight intensity enhancement near the excitation energy of 0.25 meV. The data measured at $\mathbf{Q} = (1.25, 0, 0)$ also show an increase in the inelastic-scattering intensity, although

the result is not shown here. In addition, we observed a drastic increase in intensity in the elastic scattering region of $\mathbf{Q} = (1, 0, 0)$, as shown by open marks of Fig. 1. Asymmetric spectral shape is considered to be due to alignment of four single-crystal samples. This intensity enhancement occurs below approximately 10 K. In contrast, such elastic-intensity enhancement was not observed at $\mathbf{Q} = (1.25,\ 0,\ 0)$, $(1.5,\ 0,\ 0)$, and $(1,\ 1,\ 1)$, where the signals of collective spin excitation were observed in previous zero-field INS measurements. Lower part of Fig. 1 shows a temperature dependence of the elastic-scattering intensity at $\mathbf{Q} = (1,\ 0,\ 0)$. The intensity at 1.6 K (red circles) shows a convex curve of magnetic fields, and is saturated above approximately 5 T. In contrast, the intensity at 5 K (green squares) follows a function of the squared magnetic field, as shown by a solid line fitted to the data. The data at 20 K (blue diamonds) exhibit no magnetic-field dependence. The data at 5 K indicate that the magnitude of field-induced magnetic moment shows a linear relationship to the magnetic fields, which corresponds to a paramagnetic behavior. However, the convex behavior of the data at 1.6 K is in marked contrast to the paramagnetic-like behavior. This phenomenon is rather close to that of a ferromagnetic spin correlation.

The spin correlation of the $4f$ electrons in $Ce_3Co_4Sn_{13}$, which is characterized by the signal near $\mathbf{Q} = (1,\ 0,\ 0)$, is enhanced by applied magnetic fields below 10 K. According to the study on electrical resistivity [J. R. Collave et al., J. Appl. Phys. **117**, 17E307 (2015)], the resistivity is suppressed by applied magnetic fields. This phenomenon indicates that the magnetic-field induced increase in carrier number causes a stronger RKKY-type interaction. Therefore, we expect magnetic-field tuning of the quantum criticality in the chiral-lattice symmetry of $Ce_3Co_4Sn_{13}$.

We thank P. Boutrouille for technical support on performing the neutron scattering measurements. The experiments were supported by General User Program for Neutron Scattering Experiments, Institute for Solid State Physics, The University of Tokyo, at JRR-3, Japan Atomic Energy Agency, Tokai, Japan.

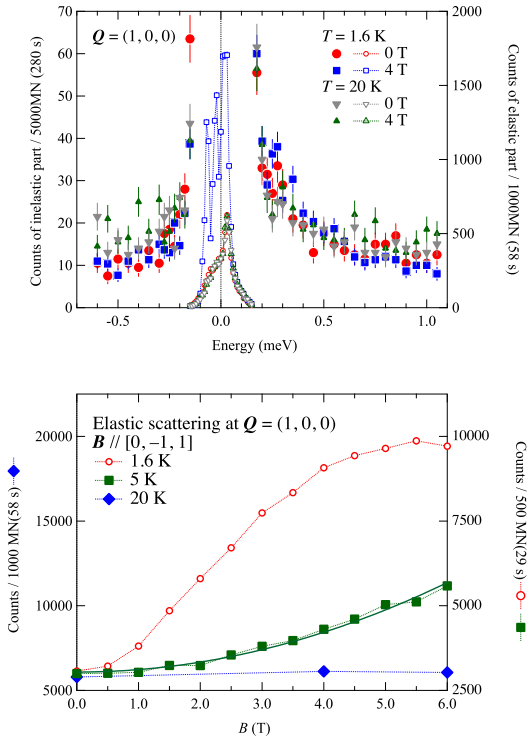

Fig. 1. (Upper part) INS spectra at $\mathbf{Q} = (1, 0, 0)$ measured at several temperatures and magnetic fields. (Lower part) Magnetic-field dependences of elastic-scattering intensity at $\mathbf{Q} = (1,\ 0,\ 0)$.

Determination of the magnetic structure in weak ferromagnetic superconductor Tb0.47Y0.53Ni2B2C

M. Takahashi(A) and H. Furukawa(A)(B)
Ochanomizu University(A), RIKEN(B)

Tb0.47Y0.53Ni2B2C is a system to show a coexistence state between the weak ferromagnetism and the superconductivity and, in such a coexistence state, one can expect to have a " spontaneous vortex phase " by an internal magnetic field mediated by the ferromagnetic components [1,2]. It is one of the issues that have not been confirmed yet. In Tb0.47Y0.53Ni2B2C, weak ferromagnetic transition temperature Twfm is higher than superconducting transition temperature Tc. With such a system, one can investigate the occurrence of the spontaneous phase without being affected by pinned vortexes.

In previous experiments, weak ferromagnetic order is confirmed below 4 K by polarized neutron diffraction experiments at HB-1 HFIR in ORNL and its magnetic structure in antiferromagnetic phase under zero magnetic field is determined as a spin density wave with a propagation vector q = 0.550a* by using a cold neutron spectrometer, CG-4C HFIR. We also measured a field dependence of a magnetic peak and found that the peak disappears above 2 T. 2 T is too small to attribute this change to saturation of the moments to the field direction. In order to investigate the change at 2 T, we performed a neutron diffraction experiment at cold neutron triple axis spectrometer MIRA, in FRM-II. The sample was mounted on a cupper plate, with a (h 0 l) scattering plane and was installed in a helium 3 insert and both of horizontal and vertical magnetic fields. Then magnetic field and temperature dependences of magnetic Bragg peaks were measured. Fig. 1 shows field dependence of a (0.56 0 0) peak in a field increasing process. There appears a difference between intensities with horizontal and vertical fields. The detailed analysis of the magnetic structure is still in undergoing.

Travel expenses were supported by General User Program for Neutron Scattering Experiments, Institute for Solid State Physics, The University of Tokyo (proposal no. 17504), at JRR-3, Japan Atomic Energy Agency.

References?

[1] H. S. Greenside, et. al., PRL 46 (1981) 49.
[2] M. Tachiki, et. al., Solid State Commun. 31 (1979) 927.

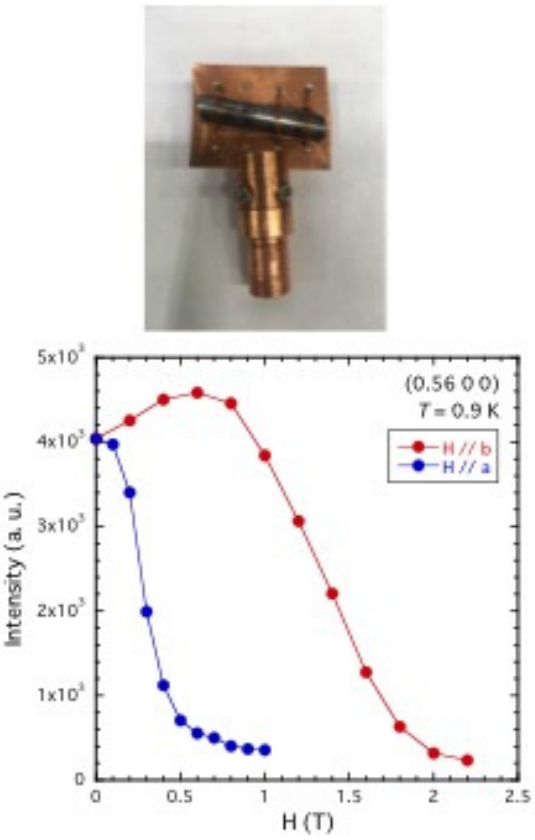

Fig. 1. A single crystal of Tb0.47Y0.53Ni2B2C and magnetic field dependence of (0.56 0 0) peak.

Neutron spin echo study on the iron-based ladder compound $BaFe_2S_3$

Y. Nambu[1], M. Nagao[2,3]
[1]*IMR, Tohoku Univ.*, [2]*NCNR, NIST*, [3]*Indiana Univ.*

Since the discovery, research on iron-based superconductivity (SC) has become the main stream in condensed matter physics. The interplay between structure, magnetism and SC is one of most intriguing subjects of this field. To gain further insight into the mechanism of SC and variation of magnetism, investigation of Fe-based compounds over distinct spatial dimensions is important. This is because the dimensionality strongly influences magnetism and can control itinerancy of electrons by changing Fermi surface topology.

We have examined magnetism of Fe-based ladder compounds AFe_2X_3 (A = Rb, Cs, Ba; X = S, Se) [1-3]. This is known as the one-dimensional analogue of the iron-based superconductors, and we have recently found the first SC in $BaFe_2S_3$ [3]. As for parent compounds of the 2D Fe-based superconductors, this 123 family shows magnetic long-range ordering. However, anomaly at the magnetic transition is invisible by bulk properties. Only neutron diffraction can determine the transition temperature. For $BaFe_2S_3$, we have clarified stripe-type magnetic structure and T_N = 119 K through powder neutron diffraction [3]. Magnetic moments (1.2 μ_B at 4 K) are arranged to form ferromagnetic units along the rung direction, stacking antiferromagnetically along the ladder direction.

However, collaborative Mössbauer experiment concludes that there is no clear transition at T_N = 119 K. Instead, there is a gradual formation of magnetic ordering, and it finally falls into the completely ordered state at 9 K, being consistent with the hindered entropy release evidenced by the specific heat data [3]. This behavior could be originating from the difference in timescale of the experimental technique; neutron has 10^{-13} to 10^{-12} sec timescale, being faster than Mössbauer (10^{-7} sec). It should be worth tracing temperature evolution of spin dynamics through the neutron spin echo technique, whose time resolution spans from 10^{-12} to 10^{-8} sec.

Neutron spin echo experiments was performed on the NGA NSE at NCNR, NIST. The incident neutron wavelength was set at λ = 5.0 Å, and shorty setup was also adopted. Data taken at 3.6 K was used as the instrumental resolution.

Figure 1 shows temperature dependence of the intermediate scattering function (ISF). The ISF shows some relaxation behavior at longer timescale and elevation of the averaged ISF as a function of temperature. This may be interpreted as the volume fraction of spins with slower dynamics beyond the given Fourier time. Together with other neutron and muon data, quantitative analysis of the dynamical magnetism in $BaFe_2S_3$ will be discussed.

[1] Y. Nambu *et al.*, Phys. Rev. B **85**, 064413 (2012). [2] F. Du *et al.*, Phys. Rev. B **85**, 214436 (2012). [3] H. Takahashi *et al.*, Nat. Mat. **14**, 1008 (2015).

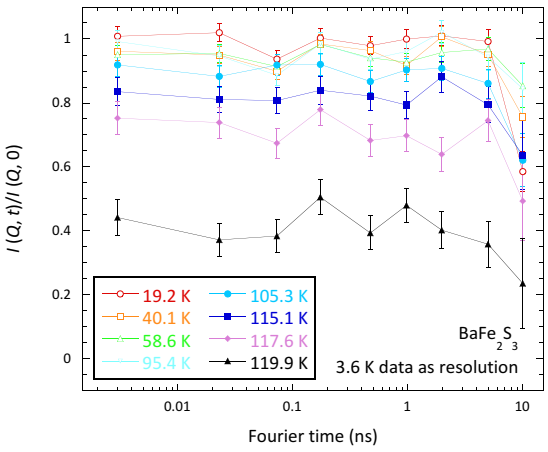

Fig. 1. Fourier time dependence of the intermediate scattering function.

Search for magnetic reflection in CeRhSn under uniaxial pressure

M. Takahashi(A), D. Okuyama(A), J. Fernandez-Baca(B), A. Aczel(B), T. Hong(B), C. L. Yang(C), M. S. Kim(C), T. Takabatake(C) and T. J. Sato(A)
(A) IMRAM Tohoku University, (B) ORNL, (C) Hiroshima University

Geometrically frustrated spin systems have been studied extensively for decades because of many intriguing phenomena, exemplified by the non-magnetic quantum disordered states. Also studied are non-magnetic ground states originating from Kondo-lattice-effect, such as those observed in Ce- and Yb-based intermetallic heavy-fermion compounds. Recently, a combination of the Kondo-effect and geometrical frustration becomes a new topic, both enhancing quantum fluctuations in different routes. This opens a new playground for the solid state physicists, and hence attracts special attention.

In this work, we study the heavy-fermion compound CeRhSn, which has a distorted kagome-lattice structure, a distorted version of a typical geometrically frustrated lattice. It has been reported that CeRhSn is indeed quite close to the quantum critical point, where divergence of quantum critical fluctuations were found below 1 K [1]. Recently, possible magnetic ordering was inferred from the macroscopic study under uniaxial pressure [2]. In this work, we search for the signal of magnetic ordering at the dilution temperature range under uniaxial pressure. The experiment was performed at CTAX cold neutron triple axis spectrometer installed at HFIR, ORNL. The hand made uniaxial pressure apparatus was used for applying pressure along the crystallographic a-axis, and the scattering was observed in the (0kl) scattering plane. Fig. 1 shows the handmade uniaxial pressure apparatus designed for this neutron experiment.

Although we thoroughly searched magnetic signal at the base temperature (roughly 150 mK) in the (0kl) scattering plane, we could not find any magnetic reflection in this plane. We presently think that the scattering plane selection was unfortunately wrong, and are now planning to repeat the same type experiment for the (hhl) plane using much high-efficiency diffractometer.

[1] Y. Tokiwa, C. Stingl, M.-S. Kim, T. Takabatake and P. Gegenwart, Sci. Adv. 2015;1 e1500001 (2015).
[2] R. Kuchler, C. Stingl, Y. Tokiwa, M. S. Kim, T. Takabatake and P. Gegenwart, Phys. Rev. B 96, 241110(R) (2017).

Fig. 1. A photograph of the handmade uniaxial pressure apparatus designed and used in the present experiemnt.

Glasses and Liquids

Dynamics of super-high entropy liquids alkylated tetraphenylporphyrins

O. Yamamuro(A), M. Nirei(A), M. Kofu(B), T. Nakanishi(C), G. Avijit(C), M. Tyagi(D)(E)
(A)ISSP-NSL Univ. Tokyo, (B)J-PARC, (C)NIMS, (D)NIST, (E)Univ. Maryland

Recently, Nakanishi group in NIMS found that large molecules, 3,5-C6C10-tetraphenylporphyrin and 2,5-C6C10-tetraphenylporphyrin, exist in liquid states at room temperature. Taking account of the fact that tetraphenylporphyrin (TPP) has a melting temperature of 723 K, the liquid phases of alkylated TPP should be stabilized by the large entropy effect which is caused by the conformational disorder of long alkylchains. This situation is similar to that of ionic liquids which are in liquid states in spite of their strong inter-ionic interactions. We call this type of liquids "super-high entropy liquids".

The purpose of this work is to clarify the dynamical feature of the alkylchains in 3,5-C6C10-TPP and 2,5-C6C10-TPP by means of QENS. This method can effectively observe the motions of alkylchains with many hydrogen atoms. Following the work on AMATERAS at J-PARC (energy resolution: 0.01-1 meV), we have carried out the QENS experiment on HFBS (energy resolution: 0.8 micro-eV) at NIST. The QENS measurements were carried out at 200, 220, 240, 260, 280, 300, 325, 350, 375 and 400 K on both spectrometers. We have combined the I(Q,t) data, which are the Fourier transformation of the S(Q,E) data, obtained by the two spectrometers. Then, the I(Q,t) data were fitted to the two KWW functions corresponding to the relaxations of alkylchains and a whole molecule (alpha-relaxation). The non-exponential parameter beta is a fitting parameter for the alkyl relaxation and fixed to be 0.5 for the alpha relaxation.

Figure 1 shows the Arrhenius plot of the averaged relaxation times and beta values. The alpha-relaxation of 2,5-C6C10-TPP is faster than that of 3,5-C6C10-TPP. This may be related to the fact that the viscosity of 3,5-C6C10-TPP (75 Pa s at 298 K) is ca. 5 times larger than that of 2,5-C6C10-TPP (16 Pa s at 298 K). On the other hand, the relaxations of alkylchains are almost the same. And the alpha-relaxation time seems to diverge at the glass transition temperature, but that of alkylchains seems to be linear and independent of the alpha-relaxation. From the Q-dependence of relaxation time, we have found that the alkylchain motion is diffusion in a confined space of ca. 0.6 nm, while the alpha-relaxation is continuous diffusion.

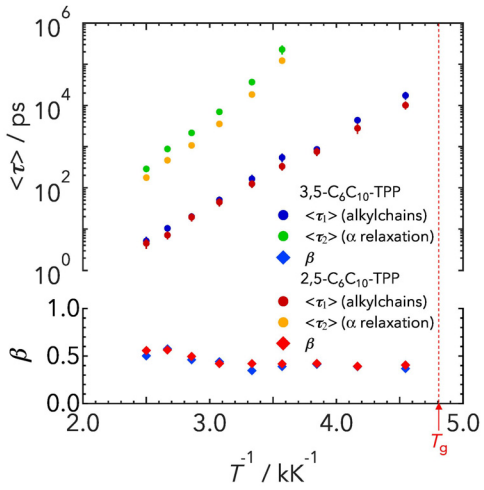

Fig. 1. Arrhenius plot of averaged relaxation times and beta values for alkyl relaxation.

Fast Dynamics of Alkylammonium-based Ionic Liquids with Plastic-crystalline Phases

O. Yamamuro(A), M. Nirei(A), M. Kofu(B), T. Yamada(C), M. Matsuki(C), M. Tyagi(D)(E)

(A)ISSP-NSL Univ. Tokyo, (B)J-PARC, (C)Kyushu Univ., (D)NIST, (E)Univ. Maryland

One of the characteristic and interesting features of ionic liquids (ILs) is nanometer-sized structure (nanostructure). For example, imidazolium-based ILs (ImILs) have nanostructures consisting of the polar-domains with imidazolium rings and anions and the non-polar domains with alkylchains of the cations. We have revealed that the nanostructure is essentially the same as that of a liquid-crystalline (LC) phase [1-3,5] and investigated the dynamics of ImILs by means of quasielastic neutron scattering (QENS) [1,2,4,5]. Recently, Yamada et al. found that some of alkylammonium-based salts, which are another popular ILs, have plastic-crystalline (PC) phases that are the counterparts to the LC phase; the LC phase has an orientationally-ordered positionally-disordered structure, while the PC phase an orientationally-disordered positionally-ordered one.

We have measured the DSC, neutron diffraction and QENS data of methyldiethylisopropyl-ammonium bis(trifluoromethylsulfonyl)imide (abbreviated as N1223 'Tf2N) and the methyl-ethylpropylisopropylammonium salt (N1233 'Tf2N) in a temperature range between 4 and 400 K. They have crystalline (C), liquid (L) and two PC phases; one may be a normal isotropic PC phase and the other an anisotropic PC phase where the cations undergo uniaxial rotations. In this work, we have conducted the QENS experiment on DCS, NIST (time range: 0.1 ps to 100 ps) following the previous experiment on HFBS, NIST (time range: 100 ps 10 ns).

Figure 1 shows the Arrhenius plot of N1233 'Tf2N obtained by both DCS and HFBS experiments; a similar result was obtained for N1223 'Tf2N. There are basically 5 relaxations in a wide time range of 4 orders of magnitude. By analyzing the Q-dependence of the relaxation times and elastic incoherent structure factors (EISF), we have succeeded to specify the relaxation modes as given in the figure.

[1] O. Yamamuro et al., J. Chem. Phys., 135, 054508 (2011). [2] M. Kofu et al., J. Phys. Chem. B, 117, 2773 (2013). [3] F. Nemoto et al., J. Phys. Chem. B, 119, 5028 (2015). [4] M. Kofu et al., J. Chem. Phys., 143, 234502 (2015). [5] F. Nemoto et al., J. Chem. Phys., in press.

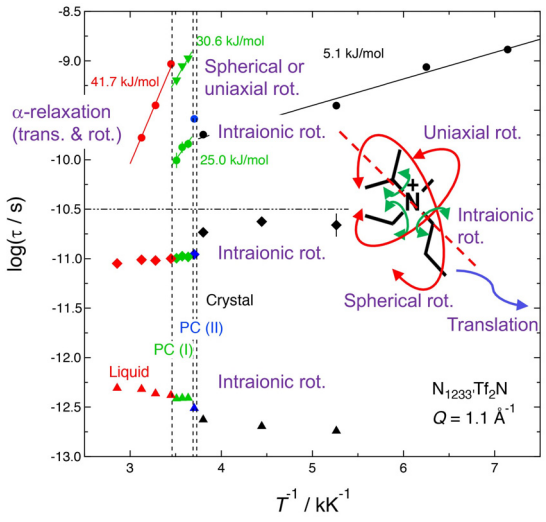

Fig. 1. Arrhenius plot of N1233 'Tf2N and assignment of each relaxation.

Dynamics of K+ aqueous solution confined in [CuZn(CN)4]- host

O. Yamamuro(A), M. Nirei(A), S. Nishikiori(B), M. Kofu(C), T. Kikuchi(C), W. Lohstroh(D)
(A)ISSP-NSL Univ. Tokyo, (B)Univ. Tokyo, (C)J-PARC, (D)Tech. Univ. Munich

Our target material is K+ aqueous solution confined in a coordination polymer host [CuZn(CN)4]-, which was recently synthesized by our group [1]. The chemical formula is [K(H2O)n][CuZn(CN)4] where n = 7.5+/-1.0. The host has nearly-spherical "cavities" of ca. 0.63 nm in a diameter. The confined K+ solution keeps electric charge balance with the negatively charged host framework. Our DSC and 2H NMR works revealed that the K+ solution in the host is not frozen at 273 K but exhibits an ordering transition at ca. 170 K and additional transitions at higher temperatures. The quasielastic neutron scattering (QENS) data taken by AGNES (JRR-3, energy resolution: 120 micro-eV) demonstrated that the motion of water molecules in the [CuZn(CN)4]- host is as fast as that of bulk water and reproduced well by the jump-diffusion model.

The aim of this study is to investigate the dynamics of water molecules more precisely, especially at low temperatures, by means of TOFTOF which has a higher energy resolution and a wider energy window than AGNES. The QENS data as functions of momentum transfer and temperature will provide important information on not only the relaxation time but also the mechanism of the relaxation. By combining the TOFTOF and AGNES data, it will be revealed how the rotational and translational motions of water molecules are activated as a function of temperature.

QENS measurements were performed at 3 energy resolution modes, 8 micro-eV (wave length: 1.2 nm), 40 micro-eV (0.6 nm), 110 micro-eV (0.5 nm), at 10 temperatures, 170K, 185 K, 200 K, 215 K, 230 K, 245 K, 260 K, 275 K, 287 K, 300 K. Clear peak broadening owing to QENS was observed at all temperatures above 185 K, indicating that water molecules diffuse in a time scale of 1 ns in the cavities of the [CuZn(CN)4]- host. This result is quite different from that of the pure water in nanoporous materials such as MCM-41 [2]; water is much slower than in the present host and exhibits a well-known liquid-liquid transition around 220 K. This may be due to the fact that K+ ions break the hydrogen-bonded network of water and enhance the mobility of water molecules.

Figure 1 presents the result of the mode distribution analysis [3] on the QENS data at 300 K. This analysis basically gives information on the number of relaxation modes and their Q dependence. There may be 1 diffusion mode and 2 or 3 more localized modes. On the basis of this result, more precise analysis on the QENS spectra is now in progress.

[1] H. Dan et al., Dalton Trans., 40, 1168 (2011). [2] L. Liu et al., Phys. Rev. Lett. 95, 117802 (2005). [3] T. Kikuchi et al., Phys. Rev. E, 87, 062314 (2013).

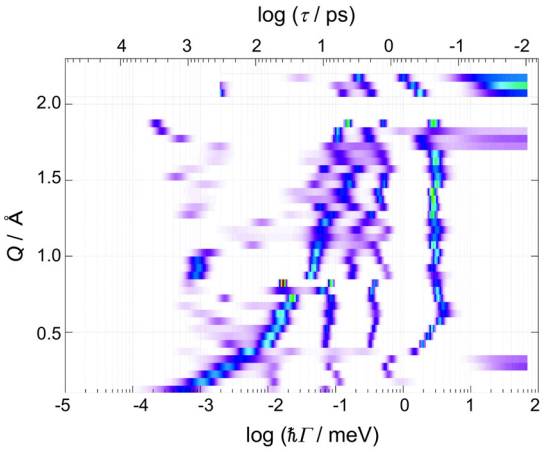

Fig. 1. Mode distribution analysis on QENS data of [K(H2O)7.5][CuZn(CN)4] at 300 K.

Biology

ATP-dependent functional domain motion of multi-domain protein MurD

Hiroshi Nakagawa (A), Michihiro Nagao (B), Tomohide Saio (C)
(A) Japan Atomic Energy Agency, (B) NIST, (C)

In structural biology, precise determination of three-dimensional structures of proteins has been focused, and the structures with an atomic-resolution have given solid platforms to understand their biological functions. Some proteins constitute multi-domains, and each domain is considered relatively rigid, while the linkers between domains brings flexibility of the molecule. It is thought that dynamical structures of multi-domain proteins link to functionally relevant phenomena, such as enzyme catalysis. Some domain motions have been explored on nanometer and nanosecond scales, where neutron spin echo (NSE) spectroscopy plays unique roles.

MurD (UDP-N-acetylmuramoylalanine–D-glutamate ligase) is a typical multi-domain protein, which is one of the ATP-driven Mur ligases that are responsible for peptidoglycan biosynthesis. The crystal structures of MurD have suggested that one of the three domains of MurD, D3, undergoes drastic conformational change from open to closed state upon ligand binding, which should control the process of the enzymatic reaction. Our recent molecular dynamics (MD) simulation showed two modes for the conformational change of D3; one " open-to-closed " and the other " rotation ". The recent NMR results suggest that the protein domain motions are significantly suppressed upon ligand binding and the proteins take a unique conformation, but no other experimental verification has been shown yet.

In this experimental report, we focus our attention on the observation of the effect of ligand binding on the domain motions of 47 kDa multi-domain protein MurD by NSE. If we successfully observe the ligand-binding related domain motions, we can understand the role of domain motions in biologically relevant functions. The experiments were carried out using NSE at NIST in USA.

We measured NSE of MurD in the ligand-bound and unbound states at a fixed temperature of T = 25 degrees C at about 60mg/ml. An incident neutron wavelength of 6, 8 and 11 angstroms was used to cover fourier times up to 100 ns in a q-range from 0.05 to 0.25 inverse angstroms. Intermediate scattering functions for both states were successfully obtained (Fig.1). The effective diffusion constants (Deff) were obtained by exponential fittings at each q. Deff should include translational and rotational diffusion as well as internal domain motions. The detail analysis on the ligand-bind dependent dynamics of MurD is on progress. We are trying to analyze the NSE data combined with computational analysis to observe the functional domain motions of MurD.

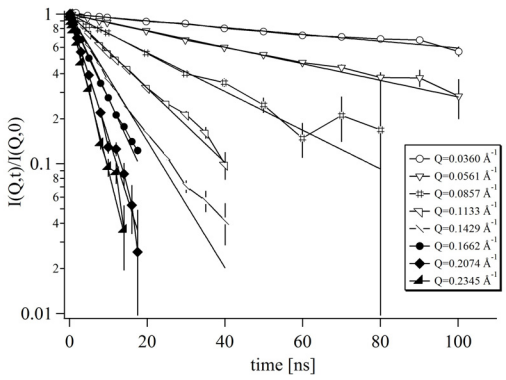

Fig. 1. Intermediate scattering function of ligand-bound MurD. Solid lines indicate the exponential fitting.

Subunit dynamics of alpha-crystallin under crowding condition

Rintaro Inoue and Masaaki Sugiyama
Research Reactor Institute, Kyoto University

In-vivo environment is highly crowded due to the presence of proteins, nuclear acids, and lipids, constituting the conditions of so-called " crowding ". One of the representative organs attaining highly concentrated system is eye lens. Eye lens are composed of three different types of crystallins, α-, β- γ- crystallin and α-crystallin is the dominant crystallin among them. α-crystallin exists as oligomers consisting of approximately 20~40 subunits. At present, the quaternary structure of α-crystallin has not been determined due to the unavailability of its crystal structure. It is considered that the failure of availability of its crystal structure might be originated from dynamical aspect of quaternary structure: " dynamic quaternary structure " induced by subunit exchange between α-crystllin oligomers. In order to reveal the mechanism of subunit exchange in α-crystllin,we applied deuteration-assisted small angle neutron scattering (DA-SANS) on α-crystallin at the concentration of ~ 1 mg/ml. On the other hand, the crowding environment is expected to be totally different from dilute system, in which the excluded volume effect or osmotic pressure is negligible. It is then postulated that the presence of close contact neighboring oligomers would alter the subunit exchange in α-crystallin. In order to mimic the crowding, we have prepared 75% deuterated α-crystllin, of whish scattering length density was estimated to be equal to 100% D2O. Fig. 1(a) shows the scattering profiles from hydrogenated α-crystallin at the concentration of 0.45 mg/ml and 75% deuterated α-crystllin at the concentration of 28 mg/ml in 100% D2O buffer. It is clearly seen that the scattering contribution from highly concentrated 75% deuterated α-crystllin is drastically suppressed in 100% D2O buffer. In order to find out the possible effect of crowding on resulting subunit exchange in α-crystllin, we have prepared two systems. One is consisted of the combination of hydrogenated α-crystallin at the concentration of 0.45 mg/ml and 75% deuterated α-crystllin at the concentration of 0.45 mg/ml in 100% D2O buffer (dilute system). The other is comprised of the combination of hydrogenated α-crystallin at the concentration of 0.45 mg/ml and 75% deuterated α-crystllin at the concentration of 28 mg/ml in 100% D2O buffer (crowding system). Both of kinetics study was performed with Quokka installed at the Australia nuclear science and technology (ANSTO) at 37 C. at the time interval of 20 min. Fig. 1 (B) and (C) shows the time evolution of forward scattering intensity (I(0)) from dilute system and crowding system, respectively. After mixing 75% deuearted α B?crystallin and hydrogenated α A?crystalline decrease of I(0) was observed, implying the existence of subunit exchange in α?crystallin. It was found that both system reached equilibrium state after 12 h after mixing. Interestingly, the exchange rate evaluated from crowding system is the same as that from dilute system within experimental error. This experimental observation reinforces our idea that subunit exchange progresses through not the collision between α?crystalline oligomers but the librated subunits. The supporting works with analytical ultra centrifuge and small angle X-ray scattering (SAXS) are on going.

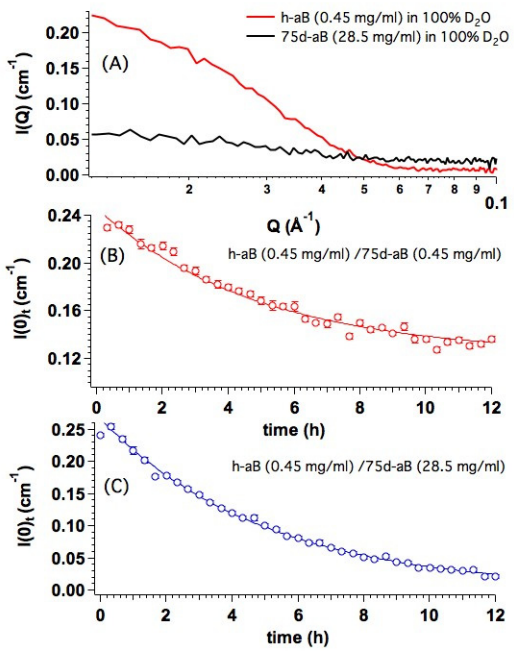

Fig. 1. (a) scattering profiles from crystallin. (b)(c) Subunit dynamics under dilute and crowding system.

Soft Matters

Quantitative evaluation of uniformity of various polymer networks by small angle neutron scattering (SANS) with contrast variation technique

Nobuyuki Watanabe1, Ken Morishima2, Xiang LI1, and Mitsuhiro Shibayama1
1 The Institute for Solid State Physics, The University of Tokyo 2 Research Reactor Institute, Kyoto University

Polymer gel is a material with flexibility and non-flowability, which has many applications in food industry and biomedical fields. The mechanical properties and swelling behavior of polymer gels depend on the network structure of the polymer gels. Recent studies by our group revealed that the influence of the homogeneity of the network structure plays a very important role on these physical properties. In 2008, our research group succeeded in fabrication of a homogeneous gel " tetra-PEG gel " by a terminal crosslinking reaction of two different types of tetra-branched poly (ethylene glycol) (Sakai et al., Macromolecules, 2008). As a result of small angle neutron scattering (SANS) measurements of tetra-PEG gel, the upturn of intensity in the small angle region, which represents the heterogeneous network structure, was not observed in tetra-PEG gel (Matsunaga et al., Macromolecules, 2009). In addition, tetra-PEG gel exhibits excellent mechanical strength and its elastic properties are well consistent with rubber theory. Although all of the scattering and rheological results support that the tetra-PEG gel is much more homogeneous than conventional polymer gels and we understand the impact of its homogeneous networks, it is still difficult to" quantitatively "evaluate the homogeneity of the structure of the tetra-PEG gels.

A method to visualize the network structure has been attempted by measuring the deuterium-labeled crosslinkers by SANS measurements with contrast variation technique. The average distance between crosslinkers were obtained in a resonable size range for various swollen conditions (Benoit, H. et al. Journal of Polymer Science 1976, 14, 2119). In this study, in order to quantitatively evaluate the polymer networks of tetra-PEG gels, Following the strategy of Benoit, we have synthesized the tetra-PEG gel with deuterium-label near the branching point and conducted SANS experiments with contrast matching method (Figure (a)). However, we failed to observe any peaks (Figure (b)). The reason is likely due to the labeled part was too small to scatter enough neutrons.

In the next study, we plan to measure a newly designed tetra-PEG gel: hydrogenated tetra-PEG polymers are crosslinked with a fully deuterium-labeled linear PEG. By using this study, the scattered intensity enough to observe and we will estimate of quantitative evaluation of uniformity of gel.

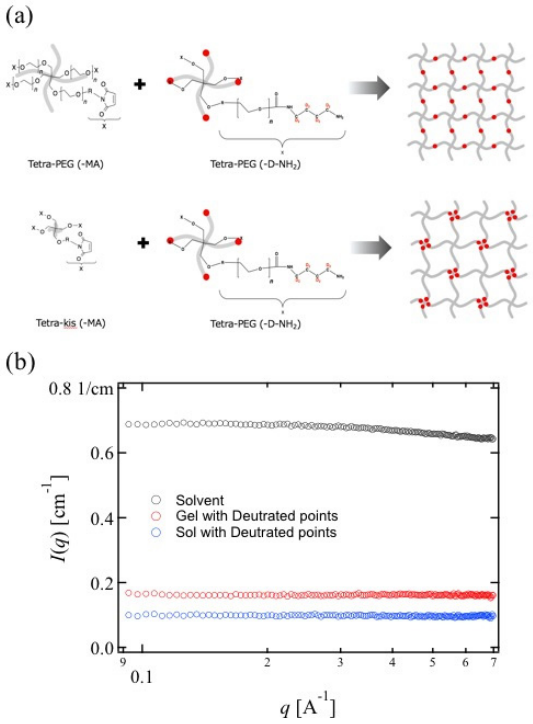

Fig. 1. (a) An illustration of tetra-PEG gels, in which deuterium atoms were introduced in the vicinity of the branching point and in the center of the branching point. (b) The result of SANS by matching contrast methods.

Structural characterization of DNA-module gel by SANS

Yusuke Yoshikawa(A), Xiang Li(A), Yui Tsuji(A), Mitsuhiro Shibayama(A)
(A) ISSP-NSL, The University of Tokyo

Physical gels (e.g. gelatin gel, agarose gel) are familiar materials in our daily life (e.g. foods, diapers). However, it is difficult to control the polymer network of them because the physical crosslinking (branching) occurs randomly and the network structure becomes very heterogeneous. In chemical gels, our group succeeded in fabrication of tetra-PEG gel, which is synthesized just by mixing two mutual reactive four-arm polyethylene glycols together (Sakai, T. et al. Macromolecules, 2008). Because the branching point in each tetra-PEG is uniformly distributed in the network, the homogeneous network will be formed. Previous our SANS study has confirmed the excellent homogeneity of networks of tetra-PEG gels (Matsunaga, T. et al., Macromolecules, 2009).

Recently, we have applied the strategy of tetra-PEG gel into physical gels by modifying the chemically reactive end-group on each arm of tetra-PEG to a physically reactive end-group: sense and anti-sense single-stranded DNA (Figure 1(a)). Because of the highly selective hydrogen binding between sense and anti-sense DNA, reproducible sol-gel transition is observed.

In this study, we carried out SANS study to investigate the temperature dependency of the structure and sol-gel transition. As the result is shown in figure 1(b), there are several interesting features. (1) No significant upturn at low-q region is observed, which suggests that this gel has homogeneous structure as conventional Tetra-PEG gel. (2) Elevating temperature, scattering intensity becomes bigger, however, no significant change was observed at sol-gel transition point (Tgel ~ 60 ℃) and the melting point of double-stranded DNA (Tm ~ 65 ℃). (3) Unpredicted peak around q = 0.02 Å-1 was observed at T > 85 ℃. The correlation distance is estimated to be ~ 30 nm, which is much larger than size of tetra-PEG polymer and that of single-stranded DNA.

In the next experiment, we plan to focus exclusively Tetra-PEG or DNA structure by using contrast matching technique. In addition, by DSC measurement along with SANS, we plan to obtain more accurate thermodynamic information of association and dissociation of double-stranded DNA.

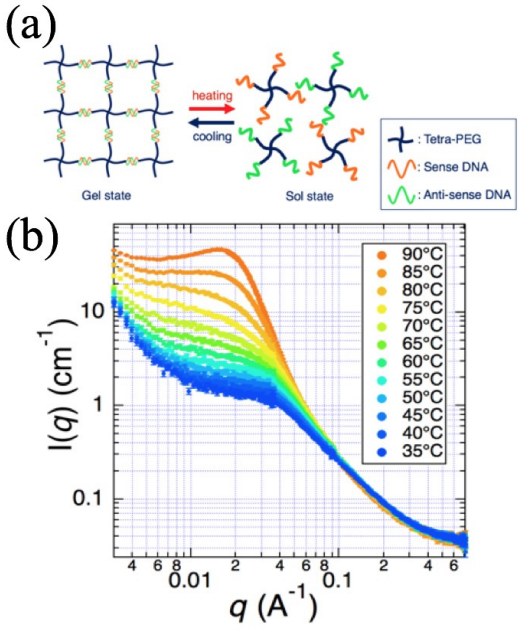

Fig. 1. (a) An illustration of DNA-module gel (b) The SANS profiles of DNA-module gel at various temperature

Structural analysis of conversion-limited critical cluster gel by small angle neutron scattering.

Takako Noritomi, Kazu Hirosawa, Xiang Li, Mitsuhiro Shibayama
The Institute for Solid State Physics

A polymer gel is a single polymer with complex three dimensional network, in which a large amount of solvent can be trapped. Polymer gels can be synthesized by various chemical methods: radical co-polymerization of monomers and cross-linkers, cross-linking the linear polymer chains by gamma-ray irradiation, coupling end-groups of star polymers, etc. Although there are many different chemical systems for various physical quantities (e.g. size-distribution, weight-averaged molecular weight, correlation length).

Recently, we established a gelation system by mixing two type of tetra-functional prepolymers, which have complementary reactive end-groups with the other type of prepolymers. In our study in ANSTO, we measured a series of critical polymer clusters by mixing these two types of prepolymers at off-stoichiometric ratio (Figure 1). With this systematic study, we have confirmed the strong universality of critical polymer clusters in in terms of fractal dimension, and for the first time found that size- distribution is actually a tunable parameter, which has been misunderstood as a universal property (Hayashi, Li et al, Nature Biomedical Engineering, 2017).

In this study, we carried out SANS study to investigate the critical clusters on way become a gel by quenching the gelation reaction near the gel point. First of all, we prepared Amine-terminated tetra-functional polyethylene glycol and N-hydroxysuccinimide-terminated tetra-functional PEG are mixed by stoichiometric molar ratio in D2O buffer(50 mM sodium phosphate, pH 3.0, 3.5, 4.0) at the various final concentration of 15, 30, 60 g/L. The reaction bath quenched near the gel point by adding small amount of HCl solution into the reaction bath to make pH close to 0, in which the reaction of amine and NHS stops. According to our previous study in ANSTO, each resultant critical solution should be diluted into different level (60, 30, 15, 7.5, 3.75, 1.88, 0.94 g/L) to fully characterize the structure and the size-distribution of the critical clusters. As the result is shown in figure 2, there are several interesting features. In the next time, we will be executed detailed analysis.

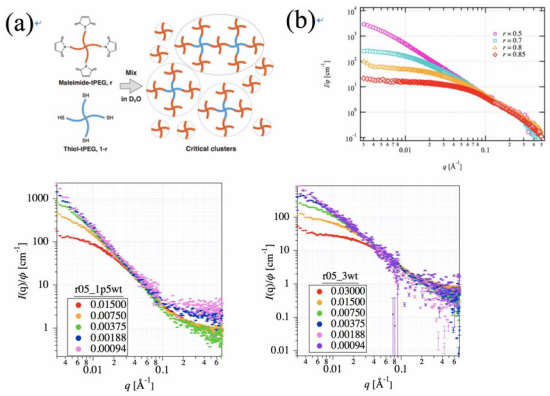

Fig. 1. Figure 1. (a) The critical clusters synthesized by imbalancing the prepolymers (b) The scattered intensities of different critical polymer clusters in previous study. Figure 2. The SANS profiles of critical cluster.

Effect of variety of alkanes on uidity and inter-lea et coupling of lipid membranes

Hatsuho Usuda[1], Mafumi Hishida[1], Elizabeth Kelley[2], Michihiro Nagao[3]
[1]*Dept. Chem. Univ. Tsukuba,* [2]*NIST Center for Neutron Research,* [3]*Dept. Phys. Indiana Univ.*

[Background] In biomembranes, various kinds of small organic molecules, such as sterols and fatty acids, regulate the physical properties of lipid bilayers to maintain cell functions. One of the typical effects of these organic molecules is on membrane fluidity, which has long been an important topic in biomembranes. Studies in biologically relevant systems have suggested that membrane fluidity affects various cell functions, such as enzyme activity, transport process, hormone action, and immune response.[1] Not only the bilayer's fluidity itself, but also the dynamic coupling/decoupling of the outer and inner leaflets of bilayers is possibly controlled by such small organic molecules. However, the effects of small organic molecules on the bilayer fluidity and the inter-leaflet coupling have not been fully understood.

The inter-leaflet coupling is known to connect the elastic bending modulus, κ, and the area compressibility modulus, K_A, in a thin elastic sheet theory.[2] As explained more in detail in the following section, recent neutron spin echo (NSE) studies start to measure both κ and K_A independently by measuring both bending and thickness fluctuations in a lipid bilayer.[3,4]

In this experiment, we investigated the effect of small organic molecules on the membrane fluidity utilizing NSE. We used synthetic lipid bilayers with and without *n*-alkanes as a model system. The effects of *n*-alkanes on the phase behavior, the bilayer structure, and its elasticity, have been extensively studied by us.[5,6] Change in the phase behavior of the lipid bilayers strongly depends on the alkane length.[5] We speculated that the membrane fluidity also relates to the intermolecular force in the membrane. For the systematic understanding of effects of various organic molecules on the membrane properties, the alkane length dependence of the membrane fluidity will be an ideal system to explore.

[Methods] The NSE technique has been traditionally used to determine membrane's elastic bending modulus, κ. However, recent development of membrane theories and experimental techniques started to shed light on more detailed membrane properties. [7,8]

Recently, thickness fluctuations in lipid membranes have been successfully measured using NSE,[3,4,9] and this technique was shown to be potential means to access β, which characterizes the interleaflet coupling.[4] The bending fluctuations have been modeled by Zilman and Granek [10] as the intermediate scattering function decays following a stretched exponential function with a stretching exponent of 2/3. The decay rate $\Gamma(q)$, where q is the momentum transfer, follows q^3 for bending fluctuations, while the thickness fluctuations are seen as a peak in $\Gamma(q)/q^3$ with an underlying q^3 dependence as follows: [4]

$$\frac{\Gamma}{q^3} = 0.0069\sqrt{\frac{k_B T}{\kappa}}\frac{k_B T}{\eta} + \frac{(\tau_{TF} q_0^3)^{-1}}{1+(q-q_0)^2\xi^2} \quad (1)$$

where the first term indicates the contribution from the bending fluctuations and the second term represents the thickness fluctuation contributions. η is the solvent viscosity, τ_{TF} represents the relaxation time for the thickness fluctuations, q_0 denotes the peak location in Γ/q^3 representation which is identical to the dip location of the bilayer form factor measured by SANS, and ξ indicates the half width at half maximum (HWHM) of the Lorentz function. The fractional change in the thickness, σ_h, is expressed as $\sigma_h = \Delta h/h = 2(q_0\xi)^{-1}$, where h represents the bilayer thickness. Neglect-

ing changes of the molecular volume, σ_h is compensated for by the fractional change in the area, σ_A, as $\sigma_h^2 = \sigma_A^2$, and a simple statistical mechanical relation connects area compressibility modulus K_A and σ_h as $K_A = k_B T/\sigma_h^2 A_0$.[11,4] Therefore, the measurement of the thickness fluctuation amplitude yields to estimate K_A. On the other hand, in a thin elastic sheet theory, a relation between κ and K_A is formulated as $K_A = \beta\kappa/d_t^2$, where d_t is the thickness of the hydrocarbon region of the membrane.[2] These two independent measure of κ and K_A by the bending and thickness fluctuations, respectively, allows one to estimate a change in β if any.

[Results] We have performed an NSE experiment on the NGA-NSE, NIST, in dipalmytoylphosphatidylcholine (DPPC) bilayers with and without alkanes. We measured the cases for *n*-octane (C8) and *n*-tetradecane (C14). We independently measured the bending and thickness fluctuations by using protiated lipid and alkanes in D_2O for the bending fluctuations, while the thickness fluctuation measurements were performed by employing tail-deuterated DPPC, deuterated *n*-alkanes and D_2O.

κ value were found to be similar for the samples with alkanes. On the other hand, strong effects of the alkanes were recognized in the thickness fluctuation measurements (Fig. **??**). $\Gamma(q)/q^3$ have peaks at lower-q for DPPC with alkanes than the pure lipid, indicating the thickness of the bilayer increased by the addition of alkanes. It is emphasized that the peak intensity and HWHM for the samples with alkanes are smaller than that for pure DPPC, and they exhibit an alkane length dependence. This implies that thickness fluctuations are depressed by alkanes, and the depression is stronger for the shorter alkane. By considering an almost constant κ but different peak width ξ, the order of the coupling constant β becomes C8<C14<pure DPPC, meaning a more coupled membrane state with alkanes, especially with the shorter alkane.

[1] J. Szöllösi, in *Mobility and proximity in biological membranes*, CRC Press (1994). Haracska, G. Bogdanovics, Z. Torok, I. Horvath, L. Vigh, *Int. J. Hyperthermia* **29**, 491 (2013).
[2] D. Boal, in *Mechanics of the Cell*, 2nd Ed.; Cambridge University Press, 267 (2002).
[3] A.C. Woodka, P.D. Butler, L. Porcar, B. Farago, M. Nagao, *Phys. Rev. Lett.* **109**, 058102 (2012).
[4] M. Nagao, E.G. Kelley, R. Ashkar, R. Bradbury, P.D. Butler, *J. Phys. Chem. Lett.* **8**, 4679 (2017).
[5] M. Hishida, A. Endo, K. Nakazawa, Y. Yamamura, K. Saito, *Chem. Phys. Lipids*, **188**, 61 (2015).
[6] M. Hishida, R. Yanagisawa, H. Usuda, Y. Yamamura, K. Saito, *J. Chem. Phys.* **144**, 041103 (2016).
[7] M.C. Watson, E.S. Penev, P.M. Welch, F.L.H. Brown, *J. Chem. Phys.* **135**, 244701 (2011).
[8] J.F. Nagle, *Phys. Rev. E* **96**, 030401(R) (2017).
[9] M. Nagao, *Phys. Rev. E* **80**, 031606 (2009).
[10] A.G. Zilman, R. Granek, *Phys. Rev. Lett.* **77**, 4788 (1996).
[11] M.P. Allen, D.J. Tildesley, *Computer Simulation of Liquids*, Clarendon Press, Oxford, 43-54 (1987).

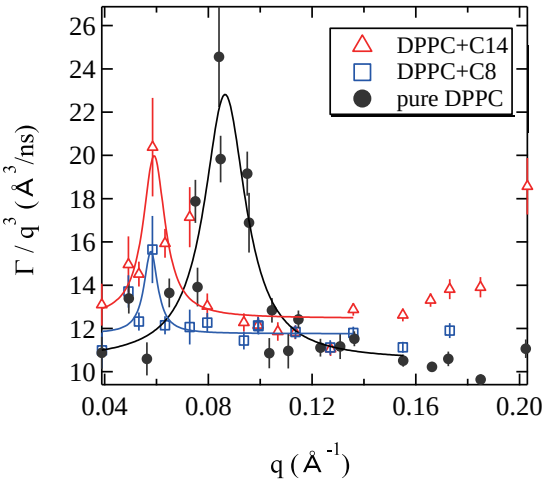

Fig. 1. $\Gamma(q)/q^3$ for DPPC with and without alkanes (C8 and C14).

Elucidation of the Mechanism of the Solvent-Dependent Switch of Helical Main-Chain Chirality of Poly(quinoxaline-2,3-diyl)s in Alkanes by Small Angle Neutron Scattering

Yuuya Nagata, Rintaro Inoue, Sota Sato, Kathleen Wood, Masaaki Sugiyama
Kyoto University, University of Tokyo, and Australian Nuclear Science and Technology Organisation (ANSTO)

Single-handed helical polymers have attracted much attention because of their applications for asymmetric catalysts, chiral stationary phase, and chiroptical materials. Recently, we developed the synthesis of helically chiral poly(quinoxaline-2,3-diyl)s (PQXs) bearing chiral side chains. Interestingly, PQXs exhibit solvent-dependent helix inversion, which can serve as effective scaffold for chirality-switchable polymer ligands and chiroptical materials. In order to reveal the mechanism of the solvent-dependent helix inversion of PQXs and control it, it is highly desirable to clarify the structural change of the PQXs before and after the solvent-dependent helix inversion.

In our previous report, we have suggested a hypothesis that conformational changes of the side chains caused by solvent effect induces the helix inversion of the PQX backbone. When the solvent could be incorporated into the side chain moiety, the side chains are extended and induce the right-handed helical conformation of the backbone. On the other hands, when the solvent could be excluded from the side chain, the side chains are shrunken and induce the left-handed helical conformation.

In this study, in order to prove this hypothesis, we focused on the temperature-dependent helix inversion of a PQX bearing (S)-3-octyloxymethyl side chains dissolved in n-octane-d18 to clarify the change of the side chain configuration by small angle neutron scattering (SANS). Before the SANS experiments, we have carried out circular dichroism (CD) measurements of the PQX dissolved in n-octane at various temperature, which exhibited the helix inversion between 313 K and 333 K. The obtained SANS patterns of the PQX dissolved in n-octane-d18 at 313, 333, 353, and 373 K are shown in the figure. Now, we are trying to reveal the conformational changes of the chiral side chains of the PQX through molecular dynamics calculations.

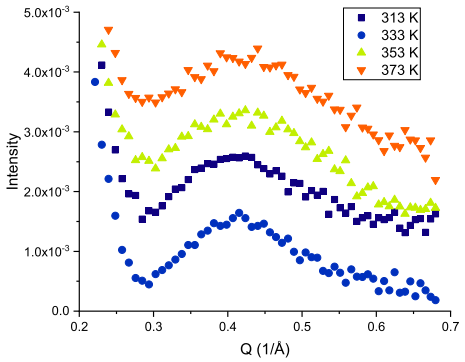

Fig. 1. SANS patterns of the PQX in n-octane-d18 at 313, 333, 353, and 373 K

Visualizing the correlation between branching point of homogeneous polymer gels

Yui Tsuji, Xiang Li, and Mitsuhiro Shibayama
The Institute for Solid State Physics, The University of Tokyo

Polymer gel is 3-dimentional network structure containing solvent. For usual polymer gel, branching point is introduced randomly. Hereby, a network structure of gel becomes heterogeneous. However, our research group succeeded in the fabrication of a very homogeneous gel recently. This gel was named " Tetra-PEG gel ". (Sakai, T. et al. Macromolecules, 2008). Tetra-PEG gel is fabricated by combining two 4-arm poly (ethylene glycol)s which are able to react mutually. It is confirmed that Tetra-PEG gels have homogeneous structure by small angle neutron scattering. (Matsunaga, T. et al., Macromolecules, 2009).

In the present study, our purpose is to quantify homogeneity of Tetra-PEG gel. For this purpose, in the previous experiment, we synthesized the tetra-PEG gel with deuterium-label near the branching point and carried out SANS experiments. However, we could not observe any peaks (Figure (a),(b)). This may be because the labeled region was too small to scatter enough neutrons.

Accordingly, we planned to measure a newly designed Tetra-PEG gel polymers were crosslinked with fully deuterated linear PEG (Figure (c)). By contrast matching of deuterated PEG, we expected to observe only the correlation peak between each hydrogenated Tetra-PEG. We fabricated 3 different concentration samples: 60 mg/mL, 30 mg/mL, and 15 mg/mL. Solutions and gels were prepared each concentration. Solutionswere prepared by combining non-reactive deuterated PEG and hydrogenated Tetra-PEG.

The observed SANS profiles are shown in the Figure (d). Open circles are solutions and filled points are gels. Peaks were not observed about solutions. On the other hand, about gel, peaks were appeared. This is because correlation appeared at a specific position with forming crosslinking. These peaks become slightly broader with decreasing concentration. This is due to incomplete network, void of network structure.

We are going to analyze this result further and write the paper.

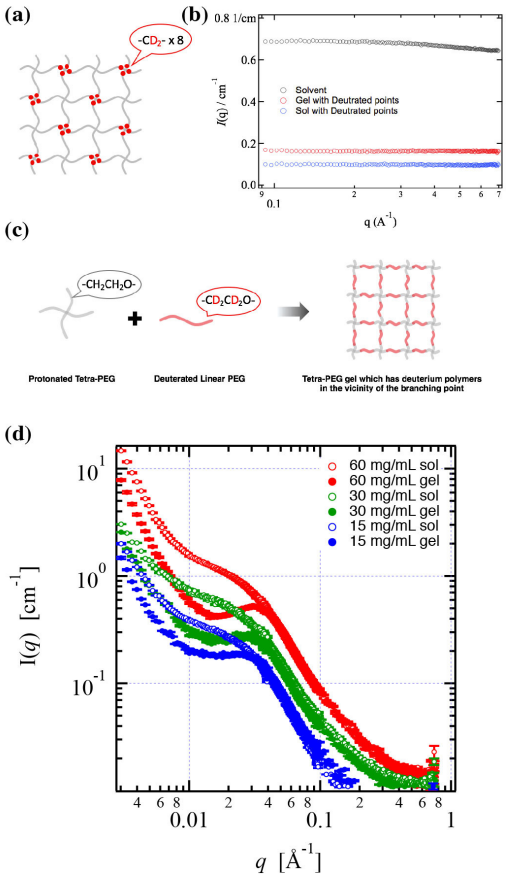

Fig. 1. (a) An illustration of Tetra-PEG gels. (b) The SANS profile in previous study.(c)An illustration of prepolymer and gels. (d)The SANS profiles of PEG gel crosslinked by deuterated polymers.

Structure analysis of metal-storing atom-mimicking dendrimers

Takako Noritomi1, Xiang Li1, Ken Minagawa2, Ken Albrecht2, Kimihisa Yamamoto2, Mistuhiro Shibayama1
1The University of Tokyo, 2The Tokyo Institute of Technology

Dendrimers are highly branched organic macromolecules with successive layers or generations of branch units surrounding a central core. They can be regarded as polymeric nanoparticles. Dendrimers exhibit internal degrees of freedom and show rich structural and dynamic features. In addition to scientific interest, dendrimers are also excellent candidates for metal accumulation carrier, and drug and gene delivery agents.

Recently, the layer-by-layer, periodically-branched structure of the dendrimer has been attracting attention because of atom mimicry, with each dendrimer generation level resembling the traditional Bohr atomic orbital（Yamamoto, K. et al.; Acc. Chem. Res. 2014, 47 (4), 1127-1136.）. Our group has succeeded in synthesizing a dendrimer ligand with this electron density gradient showing a layer-by-layer stepwise coordination, and one of these is the phenylazomethine dendrimer (DPA) (Yamamoto, K. et al.; Nature 2002, 415 (6871), 509-511). DPA is a Schiff base dendritic ligand that coordinates to Lewis acids

In this study, we carried out SANS study to investigate the dendrimers with metal ions. First of all, we added metal ions to the dendrimers. Then, we observed a difference in scattering results between samples with low and high metal concentrations in the low q-range (Figure 2). The profile in the low q-range looks rough since the scattering intensity of sample was weak. However, we observed significant difference in SANS profiles with the number of metal concentration.

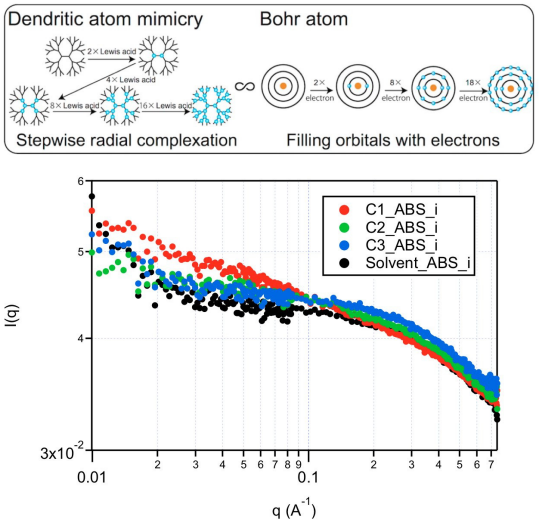

Fig. 1. Figure 1. Illustration of DPA as an atom mimicry: Comparison of the DPA and Bohr atom model. Figure 2. The SANS profiles of dendrimers